Title- Modulation of implanted aortic scaffold- involvement of ECM and immune proteins

Author's list

1. Debashish Banerjee[#] (debashish.banerjee@transplant.gu.se)

2. Nikhil B. Nayakawde (nikhil.nayakawde2010@gmail.com)

3. Deepti Antony[*] (deepti.antony@transplant.gu.se)

3. Meghshree Deshmukh[*] (meghshreed@gmail.com)

4. Sudip Ghosh[‡a] (sudip.ghosh@med.lu.se)

4. Carina Sihlbom[‡b] (carina.sihlbom@gu.se)

5. Uzair Ul Haq (qazi_raheel2003@yahoo.com)

6. Michael Olausson (michael.olausson@transplant.gu.se)

[#] Corresponding author

* and [‡] Contributed equally to this work

1, 2, 3 and 5- Laboratory for Transplantation and Regenerative Medicine, Sahlgrenska University Hospital, Gothenburg University, Sweden; 4a- Proteomic Hematology, Lund Stem Cell Center, Lund University; 4b- Proteomics core facility, Sahlgrenska Academy, University of Gothenburg, Sweden and 6 -Department of Transplantation Surgery at Sahlgrenska Academy, University of Gothenburg and Sahlgrenska University Hospital, Gothenburg, Sweden.

Keywords

vascular scaffold, decellularization, syn/allogeneic, implant, extracellular matrix, immune cells

Abstract

The development of a suitable biological scaffold or implant is a pre-requisite for the functional development of organs including blood vessels. Biological scaffold prepared by physical or chemical agents cause damage to the extracellular matrix architecture and induce immune response after scaffold implantation/engraftment. During the current study, taking advantage of different host tissue environments (subcutaneous *vs* omentum), acellular scaffolds/implants

were prepared based on syngeneic *vs* allogeneic model of scaffold implantation (*in vivo* decellularization) and compared with chemically decellularized scaffolds. Employing molecular, proteomics, and histologic techniques, we confirmed that site-specific advantages exist in modulating the ECM as well as regulating the immune responses (macrophage and T-cells) to produce an acellular scaffold without the need for immunosuppressants. The current approach opens up the possibility to create tailor-made scaffolds for further use in the clinics with a potential for long term acceptability without eliciting adverse reactions in the host. The scaffolds prepared thus would open up a further possibility to build functional organs following cell engraftment.

Impact statement

In the current study an alternative strategy of preparing a scaffold by natural means was investigated which would also give an option to avoid the detrimental effect of chemicals used while preparing a biological scaffold. Understanding the cellular milieu of an implanted scaffold would help to modify the immunological trigger upon scaffold implantation, an aspect also studied during the current research. The infiltrating cells and their putative relationship with the biological scaffold could help the researcher to target immune cells to avoid scaffold/implant rejection. In a nutshell, the study carried out without any immunosuppressive agents could help further exploration of (a) alternative strategies for preparing biological scaffolds and (b) implantable sites as potential bioreactors with the aim to avoid any adverse immune reactions for further acceptance of the scaffold/implant post implantation.

Introduction

Transplantation of organs, cells, and tissues has proved to be lifesaving by restoring essential functions e.g. normal blood flow to vital organs (e.g. coronary heart and peripheral artery disease) by revascularization techniques like angioplasty, placement of a stent, or surgical bypass scaffolding. Both synthetic and blood vessels e.g. saphenous vein, internal thoracic artery, and radial arteries are often used as a conduit for revascularization as a regenerative measure or tissue engineering approach.

The main goal for tissue engineering of blood vessels is to create vascular scaffold identical to native vessels with the potentiality to support cell engraftment. The initial development of blood vascular scaffold **[1]** and refinement in terms of rapid endothelization and extracellular matrix (ECM) deposition **[2]** has helped tissue engineering technique to develop successful blood vessels with minimum thrombosis, inflammation, and promotion of scaffold acceptance **[3, 4]**.

The usual chemical procedure used for the development of acellular biological scaffold (decellularization technology) **[5, 6]** have been reported to damage the extracellular matrix and elicit immunological reaction, immunologic incompatibility with limited mechanical tolerance **[7, 8]**. However, natural vascular scaffolds in comparison to synthetic scaffolds have certain advantages such as natural binding sites for cell adhesion (conserved native 3-D structure), improved biomimetic and biocompatibility stimulating colonization, promoting the proliferation of recruited cells. Furthermore, remodeling of the autologous vascular scaffolds *in vivo* which acquired native tissue architecture due to the maintenance of smooth muscle cells, extracellular matrix organization, and endothelial cells has been reported **[4, 9]**.

Selection of scaffold implantation sites like subcutaneous and omentum with unique cellular niche and different blood supply has been reported to support free structures for reconstructive purposes **[10-12]**. The uniqueness of the two sites for implantation has earlier been documented with the omentum rich in blood supply **[13]** whereas the subcutaneous site associated with low oxygen tensions **[14].**

Implantation of a biomaterial and its degraded by-product induces an immune reaction in the host which determines the outcome of the final integration and the biological performance of the implant. The host immune reactions following biomaterial implantation include amongst others blood-material interactions, provisional matrix formation, granulation tissue development, foreign body reaction, and fibrosis/fibrous capsule development deciding the development of acute or chronic reactions **[15].** The nature of the host immune cells e.g. macrophages depends on the immediate tissue niche of the biomaterials influencing the outcome of the tissue-specific innate and adaptive immune responses against biomaterials **[16].**

A modern scientific tool to assess biological scaffold includes mass spectrometric based quantitative proteomic analysis and bioinformatics prediction to identify and analyze proteins of the extracellular matrix **[17]** as well as an immune response after transplantation **[18].**

Based on proteomics and immunohistological tools, the dynamics of protein expression in the immediate niche of the implanted scaffolds were monitored during the current study. The findings from this study could help us to better understand the remodeling of the implant as a result of the putative interaction between the ECM and the immune infiltrating cells, chose an alternative source of implantation, as well as manipulate the immunological target to minimize adverse immune reaction.

Materials and Methods

All reagents used were of analytical grade. Antibodies used are summarized in **Supplementary tables 1A-1B.**

All animal work followed the accepted guidelines reviewed by the **local animal welfare committee at the University of Gothenburg** (Göteborgs Djurförsöksetiska Nämnd, Ethical Number, 151/14). During the current research, ARRIVE (Animal Research: Reporting of *in vivo* Experiments) and AVMA (American Veterinary Medical Association) guidelines were followed to maintain the animal welfare and care as well as improve standards of reporting (Details outlined in **Supplementary text- - Animal handling and operation).** Lewis and Norwegian Brown donor male and Lewis female recipient rats (2-2.5 months age, weight ≈180-220 g, Janvier Labs, 53941 Saint Berthevin Cedex, France) were housed and bred with food and water *ad libitum* at the Gothenburg University Experimental Biomedicine Center as per approved Animal Ethical Guidelines (Göteborgs Djurförsöksetiska Nämnd, Ethical Number, 151/14) which is regulated and governed by Swedish law and regulations, as well as by EU directives on animal welfare. A one-week acclimatisation period was given to the experimental rats to prevent stress-induced disease.

(A) Preparation of biological scaffold

Harvesting of aorta

Surgical preparation

(A) Harvesting of the donor aorta

The donor male Lewis and Brown Norway rats (n=6-8) were operated under general anaesthesia with inhalant anaesthetic, Isoflurane (which has both analgesic and anaesthetic property). A non-steroidal anti-inflammatory agent was used as pre-operative analgesia (Carprofen @5 mg/kg SC. Subsequently, the rats were subjected to induction of anesthesia in a box (receptacle) with access to anesthesia vapor using a precision vaporizer (Isoflurane - 5% in 25% oxygen at a flow of 1 l/min) leading to loss of complete consciousness and pain. Loss of pain was monitored from the absence of any writhing-type movements and pain reflexes (toe pinching) and consciousness from the absence of the definite indicators of consciousness e.g. absence of head, body and eye reflexes as a response to touch (**Supplementary text- - Animal handling and operation).** The rats were then maintained under continuous isoflurane anesthesia (3%) using a facemask when a long midline incision was performed to expose the abdominal tract, lungs and the heart under dorsal recumbence. Diaphragm was cut open to expose heart and aorta. Collection of blood was immediately performed from the heart using a 1ml syringe and a 23G needle. The branches of aorta were ligated and the aorta was

subsequently harvested. Animal was thus euthanized during the procedure of exsanguination performed under deep surgical anaesthesia. The whole operative procedure did not take more than 15 minutes to complete.

Storage of harvested blood vessel

The harvested aorta was rinsed in phosphate- buffer saline (PBS) containing antibiotic (0.5% penicillin, 0.5% streptomycin), and antimycotic (0.5% amphotericin B) finally washed with PBS and water before freezing them at -150^{0}C within 4 h of death. Aortas were thawed overnight at 4°C and used either as donor normal (normal aorta) or used for chemical decellularization before implantation as described below.

Chemical decellularization procedure of donor aorta

The decellularization steps were performed as reported earlier **[19]** at room temperature (20-24 °C) with slight modification using a closed-circuit system to minimize contamination. Each decellularization cycle consisted of a 7-hour treatment with 0.2% SDC (SDC; Sigma-Aldrich, St. Louis, MO, USA) with an alternate cycle of 7-8-hour treatment with glycerol mix solution (10% glycerol, 0.9% sodium chloride and 2 mM sodium-ethylene diaminetriacetic acid) with a wash with distilled water in between to remove cell debris as shown schematically in **Figure 1**. After the SDC cycle, washing was performed overnight with sterile water using an open system to drain out the wash continuously. A total of 5 cycles was given to achieve decellularization as assessed from DNA load and H&E staining.

Sterilization of chemically decellularized scaffold

The normal and decellularized donor aortic scaffold was sterilized by antibiotics-antimycotic solution and a pH-adjusted (pH- 7-7.4) solution of peracetic acid (2%) and ethanol (20%) for 4 hours at room temperature followed by DNase treatment as described in **Supplementary text- Methodology** (Sterilization of normal and chemically decellularized scaffolds) to achieve the recommended level of DNA load after decellularization **[20]**.

Upon confirmation of decellularization, the chemically-treated aortas were designated as decellularized aorta in comparison to the native normal aortic scaffold, referred to as the donor decellularized (DLDC/DBNDC) and donor normal (DLN and DBNN) in all subsequent sections **(Supplementary table 2).**

(B) Implantation and post-implantation biochemical study

The Lewis female recipient rats (n=6) were used for the implantation study. The recipient animal was prepared for surgery using the same indicators of pain and unconsciousness as described for the preparation of donor aorta following the same analgesic (Carpropen, 5 mg/kg bwt, SC, 20-25 min preoperatively) and anesthetic (Isoflurane- 5% in 25% oxygen at a flow of

1 l/min) procedure for induction of analgesia and anaesthesia respectively. In addition, to prevent corneal drying and trauma, ophthalmic ointment (Viscotears) was applied in both eyes and recipient animals were provided with electric heating pads during the maintenance of anaesthesia and operative procedure. The animals were operated under general anaesthesia (Isoflurane- 3% in 25% oxygen at a flow of 1 l/min). An abdominal midline incision was used for implantation of sterile implant (1.5-2 cm in length) of normal and chemically decullarized DC aortic tissue.

To minimize the number of animals, two pieces of either normal (DLN or DBNN) or decellularized donor (LDC or BNDC) scaffolds were implanted in the recipient animals. The 1st piece was implanted in the omentum, and the second scaffold was placed subcutaneous (SC). Each implant was secured with 7/0 Prolene suture and when completed, the abdominal muscle was closed with continuous suturing followed by a closure of the skin using interrupted sutures (4-0) in two separate layers. The recipient rats during the whole operative procedure was constantly monitored to avoid excessive depression of cardiac and respiratory functions, or insufficient anesthesia from the chest and flank movements. Normal pink colour of the mucous membrane was also monitored. Body temperature was also monitored with a rectal thermometer. During recovery, each animal received 1-5 ml saline (SC). Animals were placed under a heating lamp and monitored until they are fully recovered or awake. Animals were allowed to recover on paper towels in a clean cage. The rats were provided continuously supplemental heat during recovery. When the animal attained ambulatory stage it was returned to original cage with immediate access to food and water. Softened food pellets for initial few days' post-operation was also provided on cage floor.

The animals were monitored post-operative twice a day for three days with the administration of analgesics, Carpropen (5 mg/kg bwt, SC, once a day). Post-operative pain was carefully monitored by qualified staffs with knowledge of care and handling of laboratory animals. The level of spontaneous activity, back arching/ horizontal stretching, abdominal writhing, falling/staggering, poor gait and twitching, grooming, porphyrin secretions (ocular/nares), squint-eyed, pale eyes, piloerection, teeth grinding, reduced food and water intake, polyphagia of bedding and increased aggressiveness if any when handled were monitored. Any decrease in body weight (more than 10%), and deviation from the behavioural, attitudinal and physiologic signs of pain were set as an exclusion criterion for termination or sacrifice of the animal.

The recipient Lewis rats were sacrificed after two months of scaffold implantation in the same way as how donor surgery was performed. The implants from the subcutaneous and omentum

were harvested prior to sacrifice and processed for further analysis as described under **Processing of Samples**. In addition to animal groups mentioned above, we also prepared a sham group consisting of female rats of same age as the recipient animals. The sham female Lewis rats (SHAM) were prepared for surgery similar to the recipient Lewis rats, but without implantation. Hence, similar surgical intervention that included the opening and closing the abdomen with the same anaesthetics and analgesics. These rats were sacrificed at the same time points as the other recipient groups. The nomenclature of the donor as well as implanted scaffolds is outlined in **Supplementary table 2**).

Processing of samples

The donor normal, decellularized, SHAM and implanted scaffolds were stored for proteomics analysis (≈3-4 mm) and DNA isolation (≈1-1.5 mm) were snap-frozen in liquid nitrogen and stored at -150^{0}C whereas samples for gene expression (≈3-4 mm) were stored with RNALater at -80^{0}C. The scaffold samples for histological analysis (≈5-6 mm) were immediately fixed in formalin. The serum samples were prepared from collected blood and stored at -20^{0}C for further analysis.

Histological assessment

Tissue processing and staining

The donor (normal and DC) scaffolds after sterilization and implants (collected from different sites) were fixed in formalin for a period of 48 h before paraffin embedding and sectioning at 4 µM thickness. The 4 µM thickness paraffin section was deparaffinized (heating at 62^{0}C and subsequent xylene treatment), subsequently rehydrated in a decreasing grade of ethanol, and finally washed with distilled water. The sections were finally processed for H&E staining and immunohistochemical localization of different protein targets (ECM and immune cells).

Architectural preservation score of the decellularized aorta

The H&E stained sections were evaluated for structural integrity (architectural preservation) and nuclear loss (nuclear basophilia) by a pathologist (A.K.) using a Comprehensive method of masking tissues **[21]** with individual labeling of slides followed by Ordinal Data Measurements **[5].** The semi-quantitative evaluation of the tissue architecture was performed using a scoring represented as (1) complete breakdown of tissue, (2) marked disruption, 3) moderate disruption, (4) minimal disruption, and (5) no damage to cellular architecture.

Nuclear basophilia score of the decellularized aorta

A semi-quantitative nuclear loss score was performed representing nuclear basophilia (1) complete loss (100%), (2) substantial loss (70%), 3-moderate loss (50%), (4): minimal loss (30%), and (5) no loss of nuclear basophilia (0%) **[5].**

Inflammatory, fibrosis and necrosis score

To monitor the degree of inflammation, fibrosis and necrosis, a simple scoring system was used based on the following scoring criterion- (i) absent/ none-0, (ii) mild/weak- 1, (iii) moderate-2 and (iv) severe/strong- 3. Qualitative assessment for the type of inflammatory cells along with the presence or absence of any giant cell was also monitored.

Immunohistochemical assessment

Formalin-fixed paraffin sections (4 μM) were deparaffinized and subjected to heat mediated antigen retrieval for 25 min in 10 mM citrate buffer, pH 6. Sections were blocked with Candor Blocking solution+15% Normal Goat Serum for 45 min, probed with the primary antibodies diluted in low cross buffer (**Supplementary table 1)**, washed 4 times with PBS-Tween 20 (0.05%), and probed for 1h with secondary antibody, conjugated with a fluorescent probe (see **Supplementary table 1**). Finally, the air-dried slides were mounted in fluorescent mounting media containing DAPI (Fluoroshield, Cat. No. ab104139; Abcam) and imaged with a Leica Epifluorescence Microscope (DM5100). The overlapped images at 20x magnification have been shown (**Figures 7-10)** and for clarity and localization of cells 40x magnification has been presented (**Supplementary figure 11)**.

Image acquisition and analysis

The image analyses were performed using the pipelines developed by the Imaging Core Facility, Gothenburg University **(Details outlined in Supplementary text- Image Analysis).** The image analysis involved the identification of (i) the area covered by target cells (immune cells) as well as the (ii) area stained by target ECM.

During experimental acquisition, fluorescent images with 3 distinct configurations were taken named: Ch00 - nuclear staining, Ch01, and Ch02 depending on the immune markers or the ECM proteins and is specified in the corresponding figure legends.

The overlapped images have been shown for clarity and localization of the area stained for different ECM components and macrophages.

Proteomic Analysis

Sample Preparation

For proteome analysis, 3-4 mm of donor scaffolds and implants were used. In total, twelve groups were selected for proteomic analysis **(Supplementary table 2)**. The samples were homogenized in the lysis buffer (50 mM triethylammonium bicarbonate (TEAB), 2% sodium

dodecyl sulfate (SDS), centrifuged, and supernatants transferred into new vials. Protein concentration was determined using Pierce™ BCA Protein Assay (Thermo Scientific). As reference samples, the controls Donor Lewis Normal (DLN) and Donor Brown Norway Normal (DBNN) were chosen to be analyzed in both TMT sets. Aliquots containing 30 µg of each sample and the references were digested with trypsin using the filter-aided sample preparation (FASP) method **[22]**. Peptides were collected by centrifugation. Digested peptides were labeled using TMT 11-plex isobaric mass tagging reagents (Thermo Scientific) according to the manufacturer's instructions. The combined samples of each of the two TMT sets were pre-fractionated with basic reversed-phase chromatography (bRP-LC) using a Dionex Ultimate 3000 UPLC system (Thermo Fischer Scientific). Peptide separations were performed using a reversed-phase XBridge BEH C18 column (3.5 µm, 3.0x150 mm, Waters Corporation) and a linear gradient from 3% to 40% solvent B over 17 min followed by an increase to 100% B over 5 min. Solvent A was 10 mM ammonium formate buffer at pH 10.00 and solvent B was 90% acetonitrile, 10% 10 mM ammonium formate at pH 10.00. The 40 fractions were concatenated into 20 fractions, dried and reconstituted in 3% acetonitrile, 0.2% formic acid.

Liquid Chromatography-Tandem Mass Spectrometry Analysis

The fractions were analyzed on a QExactive HF mass spectrometer interfaced with the Easy-nLC1200 liquid chromatography system (Thermo Fisher Scientific). Peptides were trapped on an Acclaim Pepmap 100 C18 trap column (100 µm x 2 cm, particle size 5 µm, Thermo Fischer Scientific) and separated on an in-house packed analytical column (75 µm x 300 mm, particle size 3 µm, Reprosil-Pur C18, Dr. Maisch) using a gradient from 7% to 35% B over 76 min followed by an increase to 100% B for 8 min at a flow of 300 nL/min. The instrument operated in a data-dependent mode where the precursor ion mass spectra were acquired at a resolution of 60 000, the 10 most intense ions were isolated in a 0.7 Da isolation window and fragmented using collision energy HCD settings at either 28 or 50. MS2 spectra were recorded at a resolution of 60 000, charge states 2 to 4 were selected for fragmentation and dynamic exclusion was set to 15 s with 10 ppm tolerance.

Protein Identification and Quantification

The data files for each TMT set were merged for identification and relative quantification using Proteome Discoverer version 2.2 (Thermo Fisher Scientific). The database search was performed using the Swissprot Rat Database (Oct 2018) using Mascot 2.5.1 (Matrix Science) as a search engine with a precursor mass tolerance of 5 ppm and fragment mass tolerance of 200 mmu. Tryptic peptides were accepted with zero missed cleavage, variable modifications of methionine oxidation and fixed cysteine alkylation, TMT-label modifications of N-terminal

and lysine were selected. Percolator was used for the validation of identified proteins and the quantified proteins were filtered at 1% FDR and grouped by sharing the same sequences to minimize redundancy. Reporter ion intensities were quantified in MS2 spectra using the S/N values as abundances and normalized on the total protein abundance within the Proteome Discoverer 2.2 workflow. Only peptides unique for a given protein were considered for quantification and ratios were calculated by normalizing the samples with the reference samples DLN or DBNN. Only proteins quantified in all samples and relative standard deviation less than 25 percent in either syngeneic (LNSC, LNO, LDCSC, and LDCO) or allogeneic (BNNSC, BNNO, BNDCSC, and BNDCO) dataset were considered for comparisons among different sample groups. Proteins with two-fold expression changes were selected as up- or down-regulated.

PPI network construction and module analysis

Employing the Search Tool for the Retrieval of Interacting Genes (STRING v.10.5) **[23]**, we built the PPI network of the identified proteins. The minimum required interaction score was set to 0.400 (medium confidence), and disconnected nodes (proteins with no known interactions) were not included in the view. Moreover, the MCODE plugin of Cytoscape (v.3.7.2) **[24]** was used to identify network modules with degree cutoff = 2, node score cutoff = 0.2, k-core = 2, and max. depth = 100. The topological features of the modules were determined *via* NetworkAnalyzer **[25]** and Cytohubba **[26]** plugins of Cytoscape to identify the hub proteins. The hub proteins were mapped to the ECM and Immune responsive network modules. Pathway enrichment analyses of the networks or modules were performed through DAVID (v.6.8) **[27]** using KEGG **[28].** Benjamini-Hochberg's adjusted p-values < 0.05 were considered for statistically significant enrichment results. Gene Ontology (GO) enrichment analyses were also performed for terms related to the extracellular matrix (ECM) and immune responses.

Gene expression analysis

RNA Quantification and ddPCR

Tissue samples (scaffolds/implants) stored at -80^{0}C in RNALater were thawed, weighed, lyophilized, and cut into about 2-5 mg pieces and subjected to homogenization (4,0 m/s for 40 s, 2 cycles; Fastprep-24 5G, MP Biomedicals, CA). RNA was isolated using RNeasy micro kit (Qiagen, Cat No. 74004), measured using NanoDrop One (Thermo Scientific), integrity

assessed (Agilent RNA 6000 Pico Kit, Agilent 2100 Bioanalyzer instrument), and used finally for cDNA conversion (Cat No. 1708891; iScript cDNA synthesis kit; BioRad).

ddPCR reactions were performed using QX200 droplet digital PCR system (BioRad) and TaqMan based hydrolysis probes **[29]**. Beta actin (Actb, Rn.PT.39a.22214838.g, IDT) reference gene was used for normalization and calculation of the expression levels of the following genes: CD68 (dRnoCPE5149097, BioRad), CD163 (dRnoCPE5175377, BioRad), MRC1 (dRnoCPE5170185, BioRad) and IL-10 (dRnoCPE5172671, BioRad) **(Supplementary text - Methodology).**

Briefly, each of the 20 µL reactions contained 1×ddPCR supermix for probes (Cat. No. 1863024, BioRad), 1 µL of either FAM or HEX primer-probe mix, and 2 µL of cDNA sample (~2 ng). Each reaction was mixed with 70 µL Droplet generation oil for probes (Cat. No. 1863005, BioRad), partitioned into about ≈20,000 droplets in Cartridges for QX100 droplet generator (Cat. No. 186-4008, BioRad) and Droplet generator DG8 gasket (Cat. No. 1863009, BioRad) in QX200 Droplet Generator (BioRad), transferred to 96-well plates (BioRad) and sealed. The PCRs were performed in a C1000 Touch Thermal Cycler (BioRad) with the following cycling conditions: 1× (95°C for 10 min), 40× (94°C for 30s, 55°C for 1 min), 1× (98°C for 10 min), 1× (4°C until the plate is read) with a ramp rate of 2°C/s. The fluorescence intensity of the individual droplets produced was measured with the QX200 Droplet Reader (BioRad) after overnight incubation of the plate at 4°C. The data analysis was done with Quantasoft (BioRad) software from the negative and positive droplet population with a threshold applied manually for each well for respective genes. The target gene expression value was represented as copies/ng of input RNA as per Coulter **[30]**.

XY chromosome quantification

Tissue samples were used for DNA isolation (DNeasy blood and tissue kit, Qiagen, Cat. No. 69504) protocol, quantified using NanoDrop One (Thermo Fisher), and analyzed for detection of X and Y chromosome using X and Y chromosome-specific probes **(Supplementary text - Methodology).**

Proteome Profiler of cytokines present in serum

The relative serum cytokine expression was measured using the Proteome Profiler Rat Cytokine Array Kit, column A (R&D Systems Inc., Minneapolis, MN, ARY008 using the manufacturer's instruction **(Supplementary text - Methodology)**.

Statistical analysis

The data were statistically analyzed using GraphPad Prism v.8.4 (GraphPad Software, La Jolla, CA) and R. Differences between two groups were analyzed and p-values below 0.05 were considered statistically significant. The statistical analysis carried out in each experiment is defined in the corresponding figure legends. Details are provided in the **Supplementary text**.

Data availability

1. The experimental data required to reproduce the findings from this study will be made available to interested investigators upon request.
2. The Mass spectrometry proteomics data have been deposited to the ProteomeXchange Consortium *via* the PRIDE **[31]** with the dataset identifier PXD021179.
3. The code for all imaging pipelines for Cell and Area work will be made publicly available *via* github upon acceptance of the manuscript. During the review process we can also send the code to reviewers *via* e.g. a zip folder.

Results

The overall experimental set-up showing the preparation of an acellular vascular scaffold and subsequent implantation in recipient rats is shown **(Figure 1)**.

Decellularization strategy- Modulation of scaffolds following implantation

We initially prepared a decellularized scaffold from donor normal Lewis (DLN) and Brown Norway (DBNN) aorta and confirmed the preparation of the donor decellularized scaffolds. The load of tissue DNA measured by Picogreen assay in the decellularized scaffolds was below 10 ng and was significantly lesser (DLDC- $^{\star}p<0.05$ and DBNDC- $^{\star\star}p<0.01$) than the corresponding (donor normal scaffolds, DLN and DBNN) **(Supplementary figure 1).**

Following chemical decellularization, semi-quantitative histological scoring also confirmed significant reduction (79.31%, $p^{\star\star}<0.01$) of the acellularity or nuclear basophilia of the donor decellularized scaffolds, DLDC and DBNDC compared to the donor normal scaffolds, DLN and DBNN (**Figures 2A and 2B, Supplementary figure 2**).

Following chemical decellularization, the tissue architecture score (**Figures 2A and 2C, Supplementary figure 2**) of the donor decellularized scaffolds were reduced compared to the donor normal scaffolds. Following implantation, the omentum implants- normal and decellularized showed reduction (LNO, BNNO and LDCO - 72.41%, $^{\star\star}p<0.01$; BNDCO-

68.96, ★p<0.05) compared to the donor normal scaffolds, DLN and DBNN (**Figures 2A and 2B, Supplementary figure 2**).

The architecture of the syngeneic and allogeneic omental implants was significantly lower (LNO- 40%, p★★<0.01; BNNO- 46.67%, ★★★p<0.001; LDCO- 50%, ★★★p<0.001 and BNDCO- 43.33%, ★★p<0.01) compared to the normal scaffolds, DLN and BNN.

The subcutaneous implants (LNSC, BNSC and BNDCSC) did not show any change in the tissue architecture with the exception of syngeneic implant (LDCSC -33.33%, ★p<0.05) compared to the respective donor normal scaffold, DLN and DBNN.

There was no change in the inflammatory status of both the normal syngeneic and allogeneic implants compared to the normal donor scaffolds (**Supplementary figure 3**). However, the normal allogeneic implant, BNNO and the decellularized implants- LDCO, BNDCSC and BNDCO showed higher level of inflammatory cells, compared to the rest of the implants, which were mainly lymphocytes and later characterized immunohistologically to be macrophages. Also, there was evidence of a few giant cells in case of decellularized omentum syngeneic and allogeneic implants (LDCO and BNDCO).

Moreover, the normal allogeneic omental implant (BNNO) showed a significant increase in the fibrosis score compared to the respective normal donor implant, BNN (4.25 folds, ★★p<0.01) and normal allogeneic subcutaneous implant, BNNSC (3.4 folds, $^{\alpha}$p<0.05) respectively.

The allogeneic omental implants (BNNO- 6 folds, ★★p<0.01 and BNDCO- 5.5 folds, ★p<0.05) and decellularized subcutaneous implants (LDCSC and BNDCSC - 5-5.5 folds, ★p<0.05) showed significantly more necrosis compared to the normal donor scaffolds, LN and BLN. None of the subcutaneous implants showed significant necrosis with the exception of the syngeneic decellularized subcutaneous implant, LDCSC which showed higher necrosis score (5 folds, ★p<0.05) compared to the normal implant placed in the same route (LNSC) (**Supplementary figure 3**).

The endothelial lining was removed to a large extent even after careful washing while removing blood clots from normal rat aorta and was also not visible in the decellularized scaffolds and the implants.

Furthermore, to characterize the origin of the infiltratory cells, we performed ddPCR analysis for Y-chromosome as a marker for any donor cells present. There were negligible donor cells in the form of the Y-chromosome present in all the transplanted groups suggesting efficient natural decellularization *in vivo* **(Supplementary figure 4).**

The sham rats which received identical surgical intervention as the recipient rats showed identical DNA content and tissue architecture of aorta compared to the donor normal rats (**Supplementary figure 5).**

Proteomic analysis of syngeneic and allogeneic scaffolds following implantation

To study the differential expression of the protein after implantation, the normal and decellularized scaffolds/implants were subjected to 11-plex TMT-based LC-MS/MS-based proteomic analysis (**Supplementary figures 6A- B**). 1863 identified proteins (1% false discovery rate) were filtered for downstream analysis with a relative standard deviation of less than 25 (**Supplementary table 3**). The proteins were further analysed for the nature and reproducibility of the transplanted samples wherein we performed a principal component analysis (PCA) of the normalized protein intensity data. The implanted groups showed clear differentiation in PCA space with regards to both the route (subcutaneous, SC; omentum, O) and the nature of transplantation (syn- or allogeneic) due to homology and unique specificity (**Supplementary figure 6C**). The identified proteins also showed excellent reproducibility between replicate runs between the route and nature of transplantations (**Supplementary figure 6D**). The normal and decellularized samples of both syngeneic (Lewis-Lewis) and allogeneic (Brown Norway-Lewis) implants also significantly correlated among themselves (**Supplementary figure 6E**). The expression pattern was dynamic in the transplanted groups (**Supplementary figure 6F**). About ≈88 % of proteins were found to be common between syngeneic and allogeneic implantation suggesting maintenance of proteome stability in the transplanted scaffolds (**Supplementary figure 6G**).

Analysis of extracellular matrix protein organization after syngeneic and allogeneic implantation

ECM enriched proteins were further examined for their effect following syngeneic and allogeneic scaffold implantation at different sites. The expression of ECM proteins was quite distinct in normal and decellularized implants (**Supplementary figure 7A**). Both normal and decellularized implants shared route-specific homology. ECM proteins were significantly ($p<0.05$) enriched for GO categories related to proteinaceous extracellular matrix, extracellular matrix organization, disassembly, and extracellular fibril organization (**Supplementary figure 7B**). Furthermore, to determine the functional significance of ECM proteins in syngeneic and allogeneic set-up and to gain new insight into route-specific molecular features, we constructed

a functional interaction network with the ECM proteins and visualized in Cytoscape. Four functional modules or clusters were constructed using the MCODE plugin within Cytoscape (**Figures 3A-D**). It is evident from the cluster organization that ECM components interact with each other to maintain the ECM stability and integrity in the case of both syn- and allogeneic transplantation. In clusters 1, 2, and 4, ECM proteins interact with extracellular space proteins. Whereas in cluster 3, ECM and extracellular space proteins interact with extracellular fibril organization proteins. Some of these cluster members have a very dense connection and appears to regulate the cluster function. Ranked by degree and other 12 parameters in Cytohubba **[26]** and Network Analyzer app within Cytoscape, we identified the top eight proteins (Apoe, Apob, App, Fn1, Kng1, Sparc, Agt, and Actb) as hub proteins along with 4 relevant ECM proteins (Lamb2, Acta2, Ecm1, and Fndc1). Cluster 1 is enriched with five of the eight hub proteins (**Figure 3A**) whereas cluster 2 and 3 have one each (**Figures 3B and 3C**). These genes were Apoe, Apob, App, Fn1, Kng1, Sparc, and Agt. The heatmap represents the additional hub protein, Actb (**Figure 3E**). 5 proteins including 3 hub proteins were significantly increased in the normal syngeneic SC scaffolds, LNSC (App, Sparc, Lamb2 and Fndc1); and allogeneic SC scaffolds, BNNSC (Fndc1). In the omentum, the normal allogeneic scaffold (BNNO) showed enhanced expression for 4 proteins (Fn1, Actb, Lamb2, and Ecm1) whereas the normal syngeneic scaffold (LNO) showed 2 proteins each having either up (Sparc, Agt) or downregulated expression (Fn1, Ecm1). However, the decellularized scaffolds syngeneic (LDCO, LDSC) and allogeneic (BNDCSC and BNDCO) scaffolds showed a reduction in the expression of the ECM proteins (**Supplementary table 3, Supplementary figures 7 and 8).**

Dynamics of immune protein expression in syngeneic and allogeneic scaffolds

The proteomic data was further interrogated to evaluate the effect of immune responses in the syngeneic and allogeneic scaffolds implanted at different sites. Functional interactions for the immune-related proteins were retrieved from the STRING database. The protein expression pattern for both immune response proteins and ECM was unique for the route (subcutaneous *vs* omentum) and nature of the scaffolds (normal *vs* decellularized) implanted. Both the syngeneic and allogeneic implants at the subcutaneous site (LNSC, BNSC, LDSC, and BNDCSC) were able to keep the expression of immune-related proteins at a lower level in comparison to the omentum implants (LNO, BNO, LDO, and BNDCO). The allogeneic subcutaneous implants (BNNSC and BNDCSC) had significantly less expression level than that of the syngeneic implants (LNSC and LDCSC) for all of the immune-related proteins

except Lyn, IL6st, and CD31 (**Figure 4)**. On the other hand, the omental implants (both normal and decellularized syngeneic and allogeneic) showed more up (C1s, C4, RT1-Aw2, CD31, Serping 1, Syk and C1qa) than down (Syk, CD4, Lyn, C1qa and C1s) regulation of immune-related proteins **Figure 4)**. The majority of the immune responsive proteins showed dynamic expression and were mainly involved in the regulation of innate immune responses **(Supplementary figures 7C- 7D**). MCODE analysis resulted in the top two clusters for immune-related proteins **(Figures 4A-B)**. Cluster 1 is enriched with six of the nine hub proteins **(Figure 4A)** whereas cluster 2 has three. In cluster 1, proteins with adaptive immune response interact with proteins having the function in the regulation of immune response, which, again interact with innate immune responsive proteins in cluster 2. The 9 significantly upregulated hub proteins, as revealed by Cytohubba and Network Analyser, were Serping1, C1qb, C1s, Syk, C1qc, CD4, Lyn, C1qa, and C4. The other immune markers identified were Mpeg 1, Rt1-Aw2, Il1rap, Il6st, Cd31, and Tgfb1. Out of the 9 significantly expressed HUB proteins, 6 proteins (Serping1, C1qb, C1s, C1qc, C1qa, and C4) were related to the complement system whereas the rest 3 proteins (Syk, CD4, and Lyn) are involved in B and T-cell regulation (**Supplementary excel file**). In general, the immune proteins were not at a significantly higher level for most of the proteins detected in the implants compared to the normal scaffolds (**Supplementary figure 9)**. The number of upregulated and downregulated proteins were identical for the normal implants (6 proteins downregulated and 5 proteins being upregulated) and the decellularized implants (8 proteins downregulated and 5 proteins upregulated in comparison to the respective normal scaffolds (**Supplementary figures 7 and 9**).

Immunohistochemical localization of ECM markers following implantation

We found the presence of hub proteins from proteomic analysis including Fibronectin (Fn1), Actin (Actb), and Laminin (Lamb2) having the potential to regulate the cluster function due to their very dense connection as seen also from bioinformatics prediction. Fibronectin, laminin, and actin which also forms an integral component of the ECM were also monitored at the protein level by immunohistochemistry **(Figure 5**).

In the case of Fibronectin expression (**Figures 5A and 5B)**, significant changes were observed post-implantation in the decellularized subcutaneous implants only (LDCSC- 13.46 folds, ★$p<0.05$; BNDCSC- 7.6 folds, ★★$p<0.01$; LDCO- 15.13 folds, ★★$p<0.01$; BNDCO- 7.68 folds, ★★$p<0.01$) compared to the respective donor normal scaffolds (DLN and BNN) (**Figures 5A and 5B**). In the case of the two other ECM components, α-smooth muscle actin (**Figures 5C**

and 5D) and laminin (**Figures 5C and 5E**), the level of the ECM proteins was reduced in the donor decellularized scaffolds (DLDC and DBNDC) compared to the normal scaffolds (DLN and DBNN).

In case of the α-SMA, all the implants showed reduced expression compared to the donor normal scaffolds (DLN and DBNN) but was significantly lower in both the syngeneic and allogeneic subcutaneous implants (LNSC-19.65 folds and BNNSC-16.57 folds, ★★$p<0.01$; LDCSC-27.66 folds and BNDCSC- 19.31 folds ★★★$p<0.001$) compared to the donor normal scaffolds. The laminin expression of the decellularized implants only showed a significant reduction (LDCSC-13.68 folds, ★$p<0.05$; BNDCSC-24.15 folds, ★★$p<0.01$ and BNDCO-19.65 folds, ★$p<0.05$) compared to the respective donor normal scaffolds (DLN and DBN).

Genomic and protein expression of inflammatory markers following implantation

The proteomics findings had indicated the involvement of proteins constituting the innate immune system **(Supplementary figures 7C-D)**. Since macrophages have been indicated to play an important role in scaffold/implant acceptance, rejection or modulation, we further characterized the macrophage population at gene and protein level by digital PCR (**Figure 6)** and immunohistochemistry (**Figures 7-9**).

The genomic expression pattern of the macrophage markers- CD68, CD163 and MRC1 showed significant expression in all the implants (**Figures 6A-D**). The internal reference was β actin gene and the target gene expression was done as outlined in **Supplementary file – Methodology (Gene expression profile- calculation of target gene)** and **Supplementary figure 10.**

The level of gene expression was at a very low level in the donor Lewis (DLN) and Brown Norway (DBN) and the genes in different groups were expressed in an order CD68>CD163>MRC1≈IL10. Also, the CD68 and CD163 gene expressions of the normal subcutaneous donor implants (LNSC and BNNSC) were identical to that of the donor scaffolds irrespective of the genetic backgrounds. For the CD68 expression, the normal omentum implants (LNNO- 4.74 folds, ★$p<0.05$; BNNO-10.09 folds, ★★$p<0.01$) showed significantly higher expression compared to the donor normal and subcutaneous implants (DBNN and BNSC) (**Figure 6A**). All the decellularized implants both syngeneic (LDCSC, - 28.980 folds, ★$p<0.05$ and LDCO- 43.76 folds; p★★<0.01) and allogeneic (BNDCSC- 31.47 folds, p★★<0.01 and BNDCO- 43.73 folds; p★★★★<0.0001) implants showed significantly higher expression

compared to their respective normal (DLN and DBNN) and subcutaneous (LNSC and BNSC) implants **(Figure 6A).** Furthermore, the decellularized omentum implants (LDCO -p**<0.01 and BNDCO -p****<0.0001) had significantly higher expression compared to the normal omentum (LNO and BNNO-) implants.

The CD163 gene expression in case of the normal omental implants (LNO- 43.92 folds, p**<0.01 and BNO- 17.11 folds; p*<0.05) was significantly higher than the respective normal control (DLN and BNN).The decellularized implants (LDCSC- 57.49 folds, *p<0.05; BNDCSC- 16.24 folds; p**<0.01; LDCO- 95.92 folds and BNDCO- 45.72 folds; **p<0.01) showed significantly higher expression compared to the normal and subcutaneous implants. Also, the decellularized omental implant showed higher expression (LDCO and BNDCO, *p<0.05) compared to the normal omentum implants and decellularized subcutaneous implant (BNDCSC *p<0.05). **(Figure 6B)**.

The level of MRC-1 gene expression was very negligible in the donor scaffolds (DLN and DBNN) and was not significantly increased in case of normal implants. However, all the decellularized implants showed higher expression **(Figure 6C)**. The MRC1 expression was at a significantly higher level in the subcutaneous (LDSC, **p<0.01 and BNDCSC, *p<0.05) and omentum (LDCO- ****p<0.0001 and BNDCO-, ****p<0.0001) implants compared to the normal scaffolds **(Figure 6C).**

The anti-inflammatory cytokine, IL 10 expression was negligible in case of donor scaffolds (DNL and DBNN) and normal subcutaneous implants (LNSC and BNNSC). The expression progressively increased in the order normal omentum implant (LNO and BNNO) < decellularized subcutaneous implants (LDCSC and BNDCSC) < decellularized omentum implants. The decellularized omentum implants showed significant increase (LDCO- p**<0.01 and BNDCO- p**<0.001) compared to the respective normal scaffolds (**Figure 6D**).

We also monitored the protein level of macrophages by targeted multiplexing to characterize two protein targets by immunohistochemistry in the same tissue. We targeted to detect (i) CD68 (pan macrophage) and CD163 (M2 macrophage); (ii) MHCII (M1 macrophage) and CD163 (M2 macrophage) and (iii) iNOS (M1 macrophage) and Arginase I (M2 macrophage) in the normal scaffolds and implants by immunohistochemistry (**Figures 7-9) and Supplementary figure 11)** using validated antibodies and appropriate positive control stainings **(Supplementary figure 12).**

The expression of the pan, M1, and M2 macrophage markers was determined by dual staining and the expression level monitored as described under the **Supplementary file – Methodology**

(**Image acquisition and analysis**). The percentage of positive cells for a particular marker was expressed in terms of the nucleated cells covering particular staining area. For the pan macrophage marker, CD68 the decellularized implants (≈14-23 folds; $p^{\star} < 0.05$- $p^{\star\star} < 0.01$) and the normal implants (≈8-15 folds; $p^{\star} < 0.05$) showed significant expression compared to the normal scaffolds (**Figures 7A and 7B**).

The CD163 expression paralleled the CD68 expression albeit at a lesser level (≈2-3 folds lesser) compared to the normal scaffolds. However, there was almost identical CD163 expression of different implants (normal *vs* decellularized) placed at different sites (subcutaneous *vs* omentum) (**Figures 7A and 7C**).

Subsequently, we also monitored the expression of MHCII as a potential M2 marker in the different implants along with CD163 expression (**Figure 8**). We could detect significant increase of MHC II macrophages in the normal omentum (LNO and BNNO- 4.17-5.67 folds, $p^{\star} < 0.05$) decellularized omentum (LDCO- 8.511 folds and BNDCO- 5.295 folds, $p^{\star} < 0.05$) implants compared to the donor normal scaffolds (**Figures 8A and 8C**).

We also performed immunolabelling for two additional macrophage markers, iNOS (M1 macrophage) and Arginase I (M2 macrophage) (**Figure 9**). Significant increase in expression of M2 macrophage, Arginase I (**Figures 9A-9B**) was found mainly in the normal allogeneic (BNNO- 3.96 folds, $p^{\star} < 0.05$) and decellularized syngeneic (LDCO- 3.06 folds, $p^{\star} < 0.05$) implants. The expression of the M1 macrophage, iNOS was however weak **(Figures 9A-9C)** and was mainly observed in the subcutaneous (LNSC- 1.93 folds, $p^{\star} < 0.05$ and BNDCSC- 2.56 folds, $p^{\star} < 0.05$) implants compared to the normal scaffolds.

In addition to macrophages as part of the immune response, we also monitored T-cells ($CD3^{+}$, $CD4^{+}$, and $CD8^{+}$) infiltration in the implants by immunohistochemistry. T-cell infiltration was mainly around the implants with few cells present in the lumen of the implants (**Figure 10**). Histological observations of allogeneic and syngeneic implants revealed mainly lymphocyte infiltrations **(Figure 2 and Supplementary figure 2)**.

The expression of the pan T-cell marker, CD3+ was not significantly increased in the normal syngeneic and allogeneic implants. All the decellularized implants from the subcutaneous and omentum route showed significant upregulation of the CD3+ expression compared to the respective donor normal implants (LDCSC- 5.03 folds, $^{\star\star}p<0.01$, LDCO- 3.17 folds, $^{\star}p<0.05$; BNDCSC -6.36 folds, $^{\star}p<0.05$ and BNDCO-4.48 folds, $^{\star}p<0.05$) (**Figures 10A and 10C i**). Of the T-cell markers, CD4+ and CD8+, CD4+ was the more dominant T-cell populations (**Figures 10B and 10C ii-iii**). There was varied expression of syngeneic and allogeneic

implants at different routes of implantation (LNSC- 5.77 folds, ★★p<0.01; LNO-8.48 folds, ★★★p<0.001; BNSC-10.5 folds, ★p<0.05; BNNO- 7.50 folds, ★p<0.05; LDCSC- 8.24 folds, ★★★★p<0.0001; LDCO-8.49 folds, ★★★p<0.001; BNDCSC- 7.94 folds, ★p<0.05; and BNDCO-7.74 folds, ★p<0.05) compared to the normal scaffolds (**Figures 10B and 10C ii**).

CD8+ expression was at a much lesser level only in few groups (LNO, LDCSC and BNDCO-3.2-.4 folds, ★p<0.05) compared to the donor normal implants (**Figures 10B and 10C iii**).

We also evaluated the systemic immune response following implantation from the relative level of cytokines and chemokines using Proteome Profiler Rat Cytokine Array Kit, Panel A (**Figure 11)**. The serum from the recipient rats with normally implanted scaffolds (syngeneic – LN and allogeneic – BN) and decellularized implanted scaffolds (syngeneic – LDC and allogeneic – BNDC) was compared with a female sham (SHAM) rat for cytokine and chemokine presence at the end of 2 months. Only 5 cytokines out of 29 cytokines could be detected in the array membranes- sICAM, LIX, L-Selectin, RANTES CCL5, and CXCL7 (**Figures 11 A and B**).

However, the levels of the cytokines were fairly identical in all the implanted recipient rats and were also similar to that of the SHAM rats. The expression pattern of cytokines is probably indicative of the absence of antibody-mediated rejection following scaffold implantation.

Discussion

A current trend in the preparation of biological scaffolds for implantation/transplantation is the use of chemical decellularization technology. Despite the inherent drawbacks, biological scaffold prepared by decellularization technology has been successfully used to recreate various types of tissues and organs including the circulatory system, and subsequently repopulate with a patient's cells to produce a personalized vascular scaffold **[4, 32].**

The current work highlight the refinement in the preparation of the blood vascular scaffold using the body's natural immune response and tissue remodeling capacity in a rat model of aortic syngeneic and allogeneic implantation. As a source of the acellular scaffold, allogenic biomaterials have certain advantages such as maintenance of native tissue composition, architecture, remodeling ability, and regenerate a host tissue while circumventing the immune responses **[33]**. However, the allogeneic scaffold/implant is also encountered with adverse immune responses driven by the type and genetic mismatch of scaffolds **[34]**. The development of an acellular scaffold by natural means could help overcome the problem associated with synthetic, biological scaffolds as well as allogeneic scaffolds owing to minimizing of

unfavorable immune responses by selecting appropriate routes. During the study, we tried to utilize the body's natural ability to act as a tissue bioreactor to prepare biological implants/scaffold following implantation.

We prepared scaffold initially by chemical decellularization using an alternate cycle of SDC and Glycerol/EDTA mix to achieve an acellular state in tune with reported literature **[20]**. The chemically decellularized scaffolds showed loss of tissue architecture indicative of the deleterious effect of chemical decellularization **[35, 36].** Subsequently, we also prepared an acellular scaffold by placing aortic scaffold separately at subcutaneous and omentum sites. To monitor the fate of syngeneic (Lewis- Lewis) and allogeneic (BN- Lewis) implants following *in vivo* implantation, donor normal and decellularized/acellular scaffolds were placed as a free-floating implant with no blood vessel anastomosis subcutaneously and in omentum. The implanted scaffolds behaved uniquely according to the route of implantation with typical histological and immunological features which were monitored at the tissue level by histology, genomics and protein characterization. The omental implants irrespective of the genetic background were found in general o have a poor prognosis compared to the subcutaneous implants as evident from the architecture, fibrosis and necrosis score. The outcome was further worsened if the scaffold was decellularized prior to implantation. The presence of lymphocytes in the implants suggests the ensuing immune response to be of chronic type. However, minimum inflammation associated with the implants particularly the normal implants (except the allogeneic omentum) suggestive of favourable modulation of these implants *in vivo*. In order to monitor change in the protein expression following implantation, proteomics and bioinformatics tool along with the immunohistochemistry was used for exploring ECM and immune protein turn-over. The proteomics findings were followed by the predictive outcome of the interaction of different proteins by bioinformatics tool which indicated the involvement of unique and distinct ECM proteins present in clusters participating in the interaction with extracellular space and extracellular fibril organization proteins. The difference in nature of the scaffold and route of implantation was reflected from the hub ECM and immune proteins expression with the subcutaneous implants showing more uniform expression of ECM and immune-related proteins compared to the omentum implants. The ECM protein expression, in general, exhibited unique route-specific expression which was however not strictly dependent on the initial genetic or chemical nature of the scaffold i.e. syngeneic *vs* allogeneic and either normal or decellularized implants. The Extracellular Matrix Protein 1 (Ecm1) was up-regulated mainly in normal tissues irrespective of origin (syngeneic *vs* allogeneic). Similarly, the Fibronectin type III domain-containing protein (Fndca), which is associated with G protein

signaling was also upregulated in general. However, the ECM proteins like Fibronectin 1 (Fn1) and laminin (Lamb2) were found to be upregulated in donor syn- and allogeneic samples whereas the expression was attenuated in decellularized scaffolds. Immunohistochemical tool further showed the dynamic expression of three important ECM proteins, Fibronectin, α-SMA and laminin. Except for Fibronection, the other two ECM proteins, α-SMA and Laminin did not show increase in the expression following implantation. However, the decellularized implants showed enhanced expression of Fibronectin compared to other implants. The differential expression of ECM proteins may be the reason for the varying level of immune responses observed with respective implants. A marked increase in the expression of ECM components e.g. vascular laminins and fibronectin is a common phenomenon during early syn- and allogeneic transplantation and may trigger lymphocyte recruitment at the implantation site **[37]**. This may be the reason for the association of immune response with most of the implants studied. Also, Alpha actin (Acta2) or α-SMA which is normally associated with chronic rejection in all scaffolds **[38]** was not up-regulated in all of the implants studied. The deposition of a fibrous capsule around decellularized ECM based scaffolds which normally elicits immune response limiting tissue remodeling and regenerative potential **[6]**, was mainly limited to the normal omental implants with necrosis also observed for the decellularized omental implants with probable unresolved inflammatory responses. However, the chemical decellularization process used by us mostly preserved the ECM components as seen from the immunohistochemical data. Following decellularization, however, the ECM epitopes got exposed to the antibodies used during our experiment and were probably the reason for the higher level compared to the normal implants. Any additional enhancement in the decellularized implants could be attributed to the post-implantation modification. The proteomics findings pointed to the expression of the immune response proteins particularly the innate arm of the immune response with overlapping roles with the adaptive immune system. The immune markers detected were normally associated with complements, macrophages, and other immune cells with upregulation of the hub immune proteins in almost all the implants. However, some of the hub proteins were expressed preferentially in omental compared to the subcutaneous implants e.g. Serping1, C1qb, C1s, C1qc, C1qa, and C4, suggesting possible enhanced immune response in an omental milieu compared to the subcutaneous site. Anti-HLA class I antibodies are primarily implicated in acute rejection, whereas anti-HLA class II antibodies during late rejection. There was no upregulation in the allogeneic groups in comparison to the syngeneic scaffolds in the expression of MHC I molecules (RT1-Aw2) and

also MHC II as seen later by immunohistochemistry. The complement proteins detected by proteomics can recognize danger signals generated by foreign particles e.g. intruding pathogens or danger-associated molecular patterns (DAMPs) presented by transplanted scaffolds **[39, 40]**. Complement component, C1q e.g. plays an important role in adaptive, and innate, immunity by interacting with both immunoglobulin and non-immunoglobulin activators, surface molecules, and clearance of cell debris as part of the host defense system. The proteins like Syk, CD4, and Lyn have been implicated in the regulation of the adaptive and innate immune system. CD4, which is a membrane glycoprotein and a member of the immunoglobulin supergene family acts as a co-receptor in MHC class II-restricted T-cell activation by direct and indirect allorecognition **[41]**.

The tissue macrophages are one of the effector cells against injury and scaffold implantation carried out by modulating their own phenotype and surrounding cells. Using genomic analysis, we were able to detect pan, M1, and M2 macrophage subsets. The following subsets were detected (CD68- pan macrophage, CD163- M2 macrophage, MRC-1-M2 macrophage, and iNOS- M1 macrophage). We adapted the concept of Theoretical and Calculated ng input RNA **(Supplementary figure 10)** to normalize the reference gene which helped us to overcome the intra group variability **[30].** The target copies were then expressed in terms of the Calculated ng input RNA. Macrophages, which are an integral part of innate immune system, based on stimulation are classified as M1 (stimulated with interferon gamma, IFN-γ /lipopolysaccharide, LPS) and M2 (stimulated with interleukin-4, IL-4/interleukin-13, IL-13) macrophages. M1 macrophages are characterized by the high expression of MHC II and inducible nitric oxide synthase (iNOS) apart from the pan macrophage marker, CD68 whereas M1 macrophages are characterized by M2-associated genes such as arginase-1 (Arg1), Mrc1, CD163, and transforming growth factor beta 1 (TGF-β1) **[42].**

Genomic analysis showed that it was the decellularized implants which showed the most significant gene expression along with the normal omentum implants. The sustained gene expression could possibly explain the up regulation of protein expression seen in immunohistochemical analysis. Interestingly, two M2 marcophage lineage gene (CD163 and MRC1) along with the anitinflammatory cytokine, IL-10 expression in the implants where the modulation was found to be at the highest level, i.e. LDO and BNDCO. Using immunohistochemical means, we could identify infiltrating macrophages and their phenotypes (CD68 -pan), MHCII -M1, iNOS -M1, CD163 -M2 and Arginase -M2 as a putative immune response after implantation. We focused on the identification of mainly two broad phenotypes of macrophages - M1 (pro-inflammatory) and M2 (anti-inflammatory) which are reported to

regulate a host of inflammatory cytokines following implantation. The macrophage infiltration was predominantly located at the muscular area with fewer cells towards the lumen. The normal and decellularized omentum implants showed higher macrophage infiltration compared to the donor normal and subcutaneous implants. The pan macrophage marker, CD68 as well as the M2 macrophage, CD163 expression was more or less uniform across all the syngeneic and allogeneic at all routes. The expression for the M1 macrophage, MHCII was more prominent with the omentum implants whereas for M1 macrophage, iNOS there no uniform expression. The higher expression of MHC II in omentum implants is possibly not a favourable sign of graft acceptance which is also mirrored earlier in the histopathological changes. The level of expression for the M2 macrophage, Arginase I was also more in the omentum implants. The critical role of M2 macrophages in the remodeling of engineered vessels after implantation due to the promotion of blood vessels, cell survival, and tissue regeneration has earlier been demonstrated **[43, 44].** Even though M1 macrophages has been associated mostly with the omentum inplants, the expression of macrophages particularly the M2 subsets, CD163, Arginase I and MRC 1 could possibly indicats the type of immune response at the implantation site, a possible effort in *in vivo* to facilitate favorable remodeling of the implanted scaffolds without rejection.

An elevation of inflammatory markers and immune cell circulation has been reported as one of the main causes of all scaffold rejection promoted us to characterize tissue distribution of T-lymphocytes after implantation. To monitor the dynamics of the T-cell mediated rejection of implanted tissue, the presence of CD4+, CD8+ lymphocytes were detected along with the pan T-cell marker, CD3+ cells. Earlier CD4 protein was detected as a hub protein by proteomics. Moreover, the CD4+/CD8+ ratio is usually increased after solid allogeneic/alloscaffold transplantation and is an important index for evaluating immune rejection [45, 46]. Our study showed that the CD4+ and CD8+ cells in the syngeneic and allogeneic scaffolds were almost at an identical expression level. The presence of identical immune markers having the identical expression level after implantation of syngeneic and allogeneic scaffolds suggests the involvement of a sterile inflammation at the implantation site which is produced irrespective of the genetic backgrounds. A statistically significant increase in the CD3+ cell was observed in all the decellularized implants whereas an increase of CD4+ cells with a minimum infiltration of CD8+ cells was observed in both the normal and decellularized implants, suggestive of an absence of a strong T-cell-mediated immune response. The cellular infiltration reveals the nature of the infiltrate which is mainly CD4+ suggesting a delay in the rejection process but an window of opportunity to create a biological scaffold with maintenance of

essential ECM components. Both the syngeneic and allogeneic implants showed well-preserved smooth muscles of blood vascular architecture and minimum intralumen cellular infiltrate with predominant mononuclear cell infiltration confined to the periscaffold space. Statistically significant increased proportion of CD4+ T-lymphocytes in the implanted scaffolds when compared with donor normal scaffolds as observed in our case could lead to improved scaffold outcome after implantation as has been reported with allogeneic transplant acceptance **[47].** The immune responsive proteins were mostly upregulated in normal allogeneic omental implants suggestive of a more localized immune response in the omentum. In syngeneic transplants, the pattern was quite distinct, with normal syngeneic transplants showing upregulated immune responsive proteins in comparison to the decellularized syngeneic transplants which showed down-regulated immune response proteins. We have seen earlier from gene expression study the increased expression of the anti-inflammatory cytokine, such as IL-10 in those scaffolds where there was consistent macrophage infiltration (LDCO and BNDCO), is suggestive that these implants were also possibly protected from damage due to excessive inflammation made possible due to potential crosstalk with a subpopulation of T cells such as regulatory (Tregs) **[48, 49]**.

In terms of the systemic immune response, there were no serum markers suggestive of any systemic inflammatory response. All the detected immune markers were found to be at the same level as the SHAM operated rats supporting a more favorable outcome of scaffold remodeling. We observed immune responses which were of moderate grade and were not severe to destroy the scaffold after implantation. This observation probably could be attributed to the anatomical feature of the blood vascular scaffold aorta having a large diameter, a marked absence of endothelial lining even during gentle processing, the rigidity of the vessel as well as the implantation route selected. The subcutaneous site allowed minimizing the ensuing immune responses whereas the omentum prompted a more vigorous immune response which leads to alteration in the tissue architecture of the scaffold. The chemical decellularization strategy used was aimed to minimize the tissue architecture damage in terms of the ECM or triggering of an adverse immune reaction, which was to some extent again circumvented by choosing the subcutaneous route for implantation. The host response at different sites was similar to non-resorbableble foreign material characterized by low-grade chronic inflammation, negligible scaffold degradation and or necrosis and fibrosis was supported by our histology and immunohistological findings. The differential responses of tissue scaffolds placed subcutaneously **[50]** and in the omentum **[51]** have been reported earlier and points to the presence of innate immune cells particularly macrophages in the vicinity of the scaffold

which could have contributed to the acellular state of both the syngeneic and allogeneic scaffolds placed at these routes during our study.

Biological scaffolds based on ECM have been shown to normally promote a macrophage switch from M1 to M2 cell population deciding the outcome of post-implantation. However, chemical decellularization can expose the ECM preventing the beneficial M2 response which can lead to scar tissue formation **[52, 53].** Moreover, alteration of the tissue-specific ECM composition following organ transplantation has also been reported **[54]**.

So, we decided to compare an acellular scaffold/implant prepared without the involvement of chemicals but rather harnessing the body's natural immune defense system, which was in our case predominantly the innate arm of the immune system i.e macrophages and partly adapted immunity through the involvement of $CD4^+$ T-helper cells. From our histological findings, we could conclude that there was mostly maintenance of the typical smooth muscle architecture as well as the absence of a fibrous capsule around the normal and decellularized implants. However, we did not further process the normal aorta or the chemically decellularized aorta for further anastomosis study but rather used them to evaluate the alteration of the scaffold/ECM and ensuing immune responses after implantaton. A functional evaluation of the prepared biological scaffolds by natural means vis-à-vis chemically modified scaffolds is a future option that we would like to explore.

Concluding statement

The study opens up the possibility to utilize nature's immune machinery to produce an acellular scaffold that has the potential to support cellular support and growth due to the maintenance of ECM components as well as triggering moderate immune reactions after implantation. The importance of the development of a natural biological scaffold also stems from the concern with the fast commercialization of tissue-engineered organs e.g. decellularized tissue for clinical application in humans by FDA and CE which could possibly jeopardize patient's safety on the grounds of quality control and safety of transplantable organs **[55].** There are few limitations to this study though. Our study was based on a terminal time point of 2 months which did not allow for dynamic observations. We only used our implant as a free-floating scaffold without direct blood vascular anastomosis, limiting the potential of our developed scaffold as a graft. However, the main motive of our study was to develop a biological scaffold and to study the response of body's natural immune machinery against different implants at two pre-decided implant sites and to observe the remodeling events subsequent to implantation.

Author contributions

Debashish Banerjee: Conceptualization, Methodology, Investigation, Writing - original draft **Nikhil B. Nayakawde:** Conceptualization, Methodology, Investigation. **Deepti Antony, Meghshree Deshmukh, Sudip Ghosh and Carina Silbohm:** Methodology, Investigation **Uzair Ul Haq:** Methodology and **Michael Olausson:** Methodology, Supervision, Funding acquisition.

Acknowledgments

The authors would like to thank Rafael Camacho, Center for Cellular Imaging, University of Gothenburg for developing the image analysis pipelines and Dr. Anikó Kovács (A.K.), pathologist, Sahlgrenska University Hospital, University of Gothenburg for the Histological interpretation.

Funding Information

The research was financed by the Swedish Government LUA ALF and IngaBritt och Arne Lundbergs Forskningsstiftelse grants to Michael Olausson and Stiftelsen Professor Lars-Erik Gelins Minnesfond grant to Debashish Banerjee.

The funders had no role in the study design, data collection and interpretation as well as the decision to submit the work for publication.

Data availability

1. The raw/processed data required to reproduce few of the findings could not be shared at this time due to technical or time limitations. The experimental data required to reproduce the findings from this study will be made available to interested investigators upon request.
2. The Mass spectrometry proteomics data have been deposited to the ProteomeXchange Consortium *via* the PRIDE **[31]** with the dataset identifier PXD021179.
3. The code for all imaging pipelines for Cell and Area work will be made publicly available *via* github upon acceptance of the manuscript. During the review process we can also send the code to reviewers *via* e.g. a zip folder.

Declaration of interests

The authors declare that they have no known competing financial interests or personal relationships that could have appeared to influence the work reported in this paper.

Figure and Figure Legends

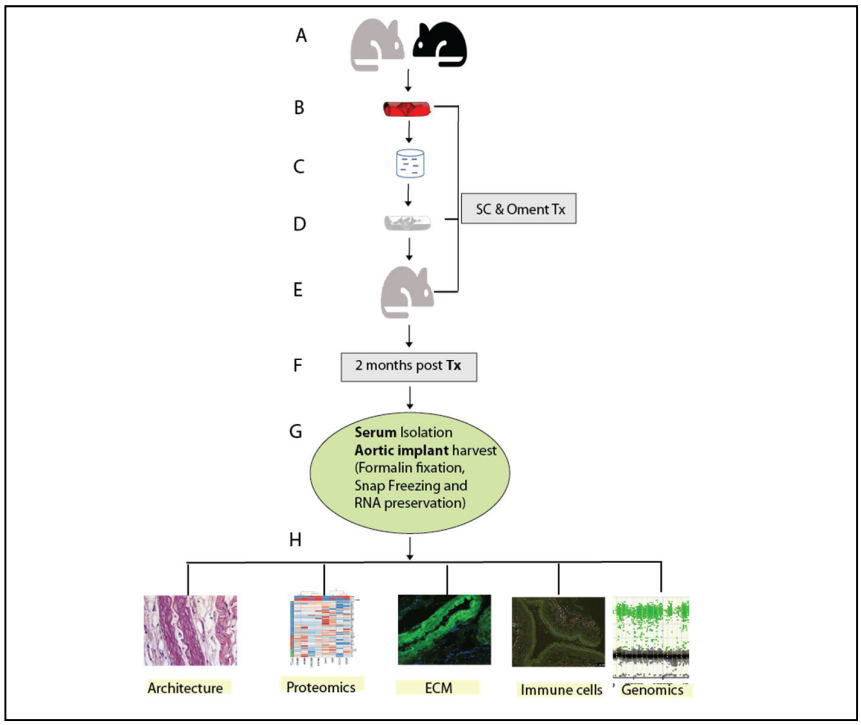

Figure 1. The experimental design and layout of the study. The experimental design is presented in a sequential layout **(A-H)**. Male Lewis and Brown Norway donor rats **(A)** were used for harvesting the aorta **(B)** as described in the Materials and Methods section. The aortas from donor rats (male Lewis/Brown Norway) were then perfused with chemical solution **(C)** to prepare a decellularized aortic scaffold **(D).** Implantations of the normal donor aorta **(B)** and decellularized aortas **(D)** at subcutaneous and omentum route were performed in female recipient mice **(E).** The implanted aortas and serum were collected following sacrifice of the recipient mice after 2 months, **(F)** for downstream processing for serum and tissues, **(G).** The tissue architecture, proteomics, ECM and genomic characterization were performed, **(H).**

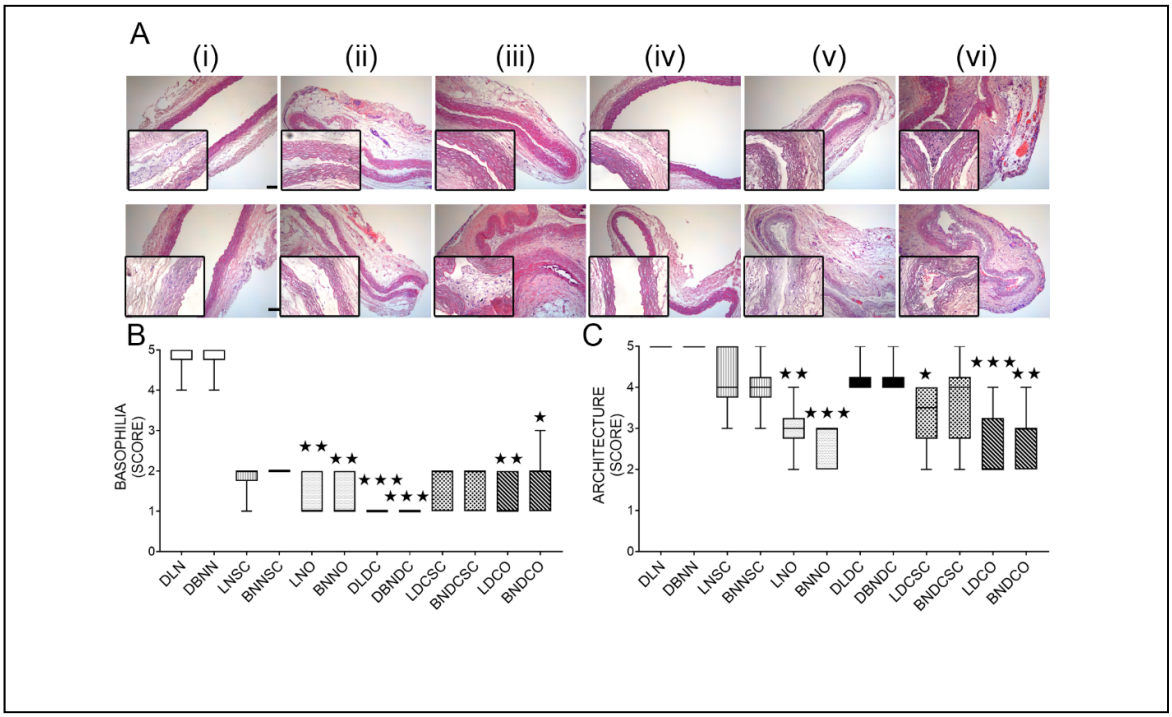

Figure 2. H&E staining of normal and decellularized scaffolds before and after subcutaneous and omental implantation.

(**A**). Upper panel- Lewis (L) and lower panel- Brown Norway (BN) donor normal and decellularized scaffolds and after implantation and harvest from subcutaneous and omentum route after 2 months. (i) normal (N), (ii) normal subcutaneous (NSC) (iii) normal omentum (NO), (iv) decellularized (DC), (v) decellularized subcutaneous (DCSC) and (vi) decellularized omentum (DCO). All the donor scaffolds were stained with H&E and compared to the implanted aortas in terms of the Nuclear basophilia (**B**) and Architectural score (**C**) as defined in the Materials and Methods section. Representative images are shown at 10× magnification. Scale bars: 100 µm~~. (n=6 in each group).~~ Results are presented (n=6 in each group) as maximum and minimum of the rank. (median in the middle of each box). ★$p<0.05$, ★★$p<0.01$ and ★★★$p<0.001$ indicates a significant difference in

comparison to the respective normal donor aorta by Kruskal-Wallis test followed by Dunn's Multiple Comparisons post hoc tests.

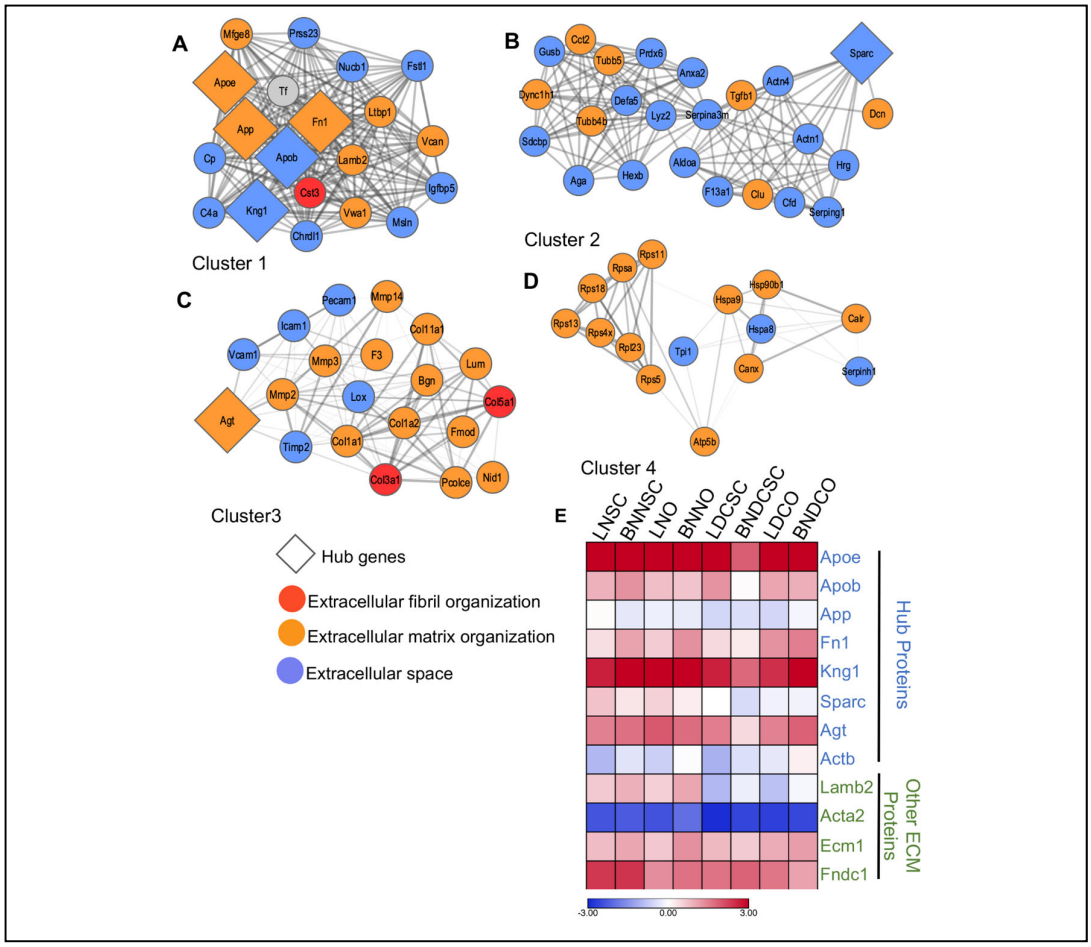

Figure 3. **The topological features of the ECM Network.**

The PPI network of the 8 hub and related proteins, created by quering the proteins enriched for ECM function against the STRING database. The network was exported and visualized using cytoscape. Proteins were then clustered with MCODE algorithm. Hub proteins were identified using Cytohubba app within the Cytoscape (A-D) MCODE cluster 1-4 respectively. Node color represents gene ontology terms and the edge width was proportional to the combined score based on STRING database. (E) Protein expression dynamics of the hub and selected ECM proteins showing heterogeneity within the transplanted groups. The colour scale represents the log2 normalized expression values.

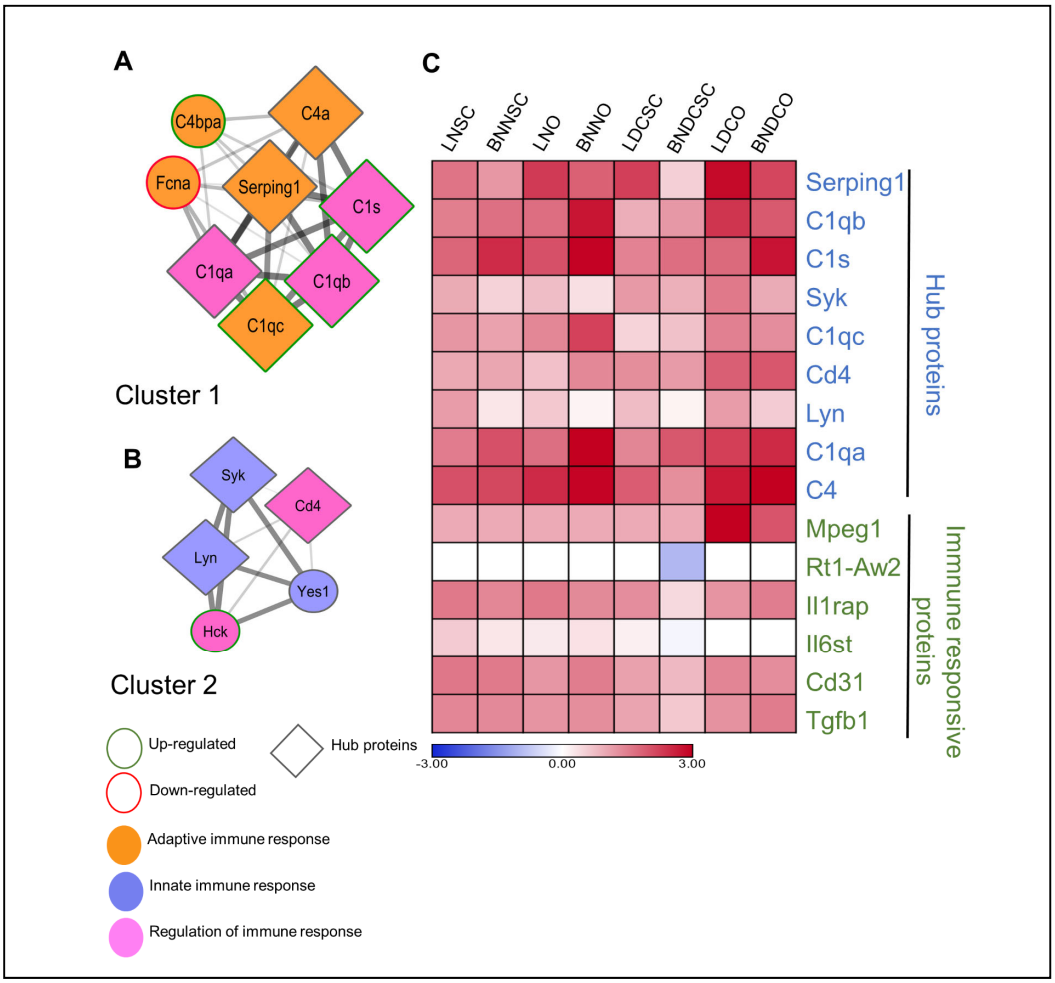

Figure 4. PPI network integration of the immune responsive proteins.

The PPI network was created by quering the proteins enriched for immune function against the STRING database. Network relationships derived from the STRING database were visualized with cytoscape. Proteins were then clustered with MCODE algorithm. Hub proteins were identified using cytohubba app within the cytoscape. **(A, B)** The top 2 MCODE clusters. Each node represents a protein and each edge denotes an interaction between a pair of proteins. Node color represents gene ontology terms and the thickness of the edge represents a larger combined-score derived from STRING database. **(C)** Protein expression dynamics of the hub and selected immune responsive proteins showing heterogeneity within the transplanted groups. The colour scale represents the log2 normalized expression values.

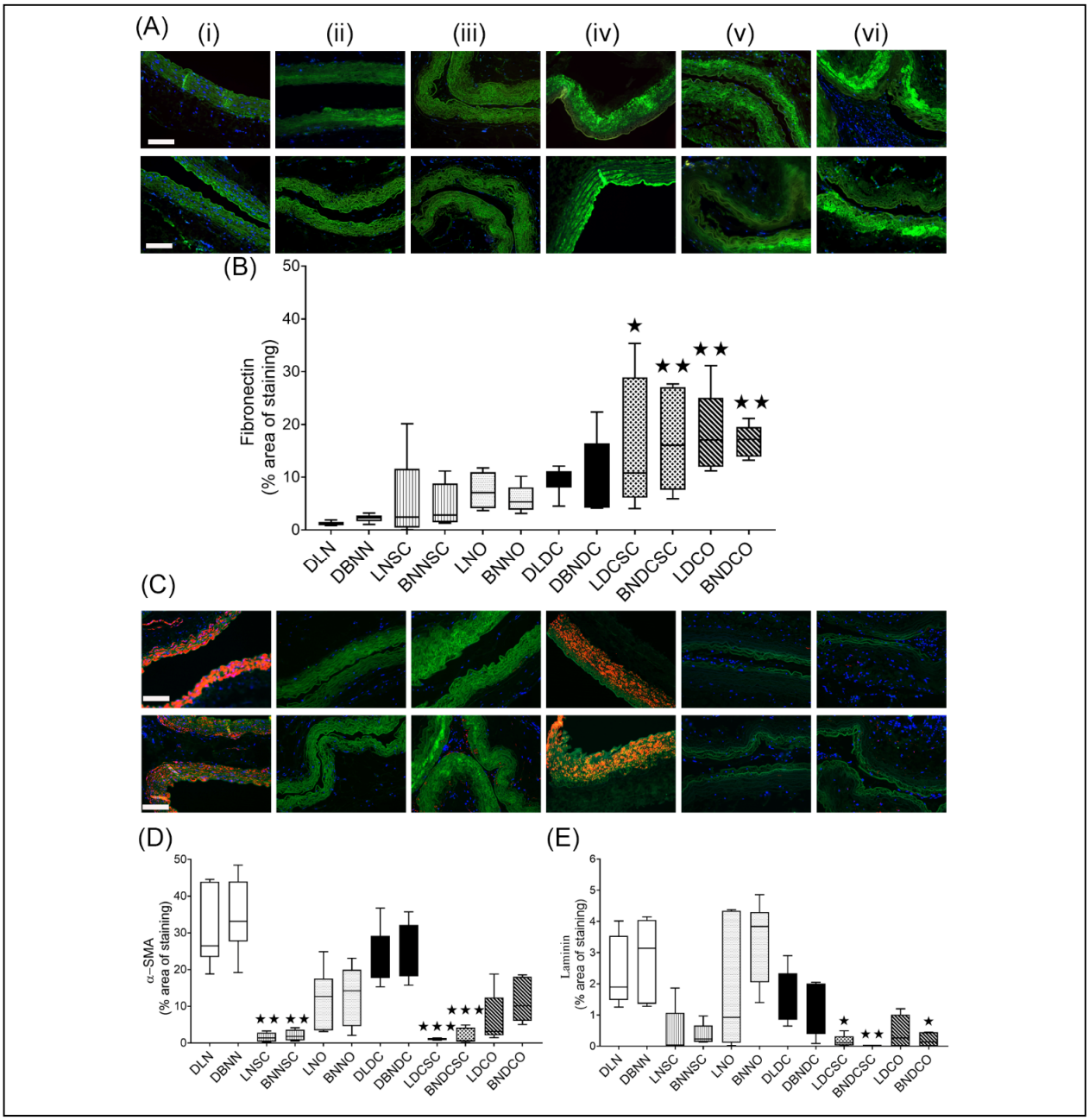

Figure 5. Immunohistostaining identifying expression of different ECM components following implantation of aortic scaffolds.

Implanted scaffolds after 2 months' time period were analyzed by histological assessment of different ECM components as outlined in Materials and Methods section. The upper panel denotes the implants from Lewis (L) and lower panel from Brown Norway (BN) rats respectively. (i) normal (N), (ii) normal subcutaneous (NSC) (iii) normal omentum (NO), (iv) decellularized (DC), (v) decellularized subcutaneous (DCSC) and (vi) decellularized omentum (DCO).

A- Localization and B- Quantification of Fibronectin (green colour).

C- Localization and D-E- Quantification of α-SMA (red colour) and Laminin (green colour).

Representative images are shown at 20x magnification. Scale bars: 100 μm.

Results are presented (n=6 in each group) as maximum and minimum of the rank (median shown in the middle of each box).★p<0.05 and ★★p<0.01 and ★★★p<0.001 indicates a significant difference in comparison to the respective normal implants by Kruskal-Wallis test followed by Dunn's Multiple Comparisons post hoc test.

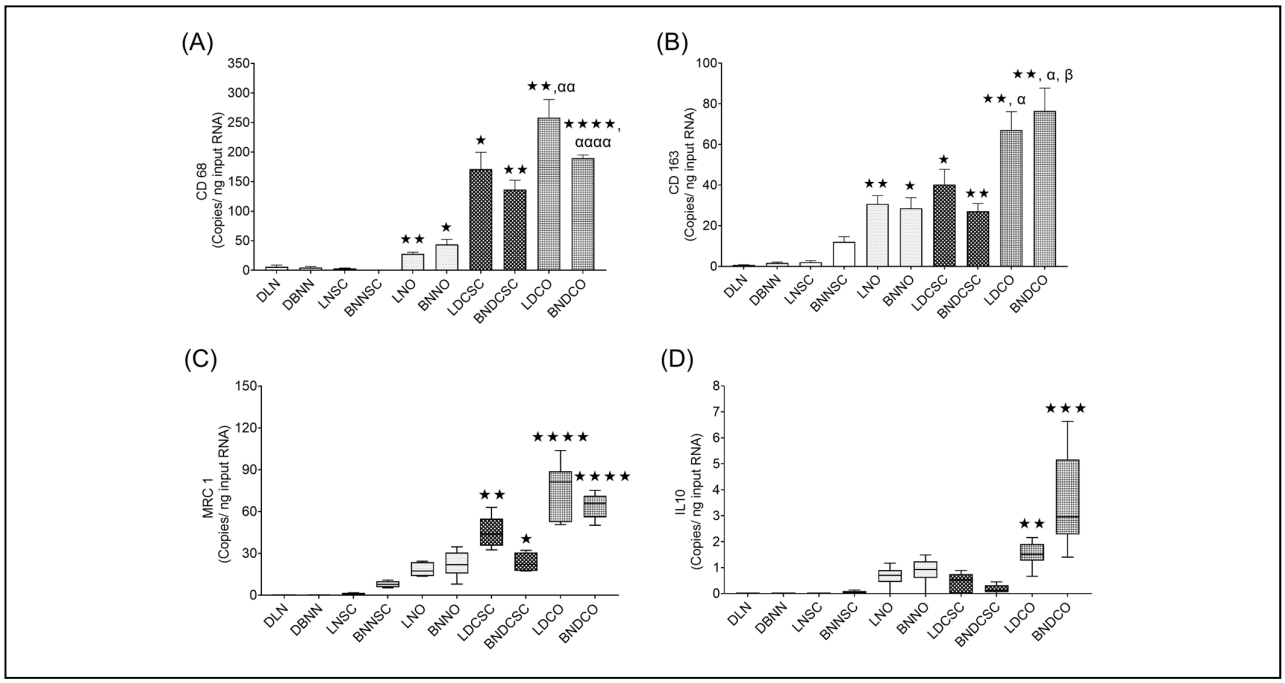

Figure 6. Gene expression analysis of different macrophage subsets following implantation.

Implanted scaffolds after 2 months' time period were characterized for gene expression of different macrophages (M1 *vs* M2 subsets).

A-E. Copies per ng input RNA of macrophage target gene were calculated using theoretical concentration of the target gene using reference gene, β-actin as outlined in the Materials and methods section. Data are shown as median and range of values (n=6 in each group).

A-B. Results are shown as Mean±SEM (n=6 in each group). ★p<0.05, ★★p<0.01, ★★★p<0.001 and ★★★★p<0.0001 indicates a significant difference compared to the respective donor normal scaffold and normal subcutaneous implants; αp<0.05, ααp<0.01 and αααp<0.0001 indicates a

significant difference in compared to the respective normal omentum implants and $^{\beta}p<0.05$ indicates a significant difference compared to the respective decellularized implant by One-way ANOVA followed by Dunnett's T3 Multiple Comparisons post hoc test.

C-D. Results are presented (n=6 in each group) as maximum and minimum of the rank (median in the middle of each box). $^{\star}p<0.05$, $^{\star\star}p<0.01$, $^{\star\star\star}p<0.001$ and $^{\star\star\star\star}p<0.0001$ indicates a significant difference compared to the respective donor normal scaffolds by Kruskal-Wallis test followed by Dunn's Multiple Comparisons post hoc test.

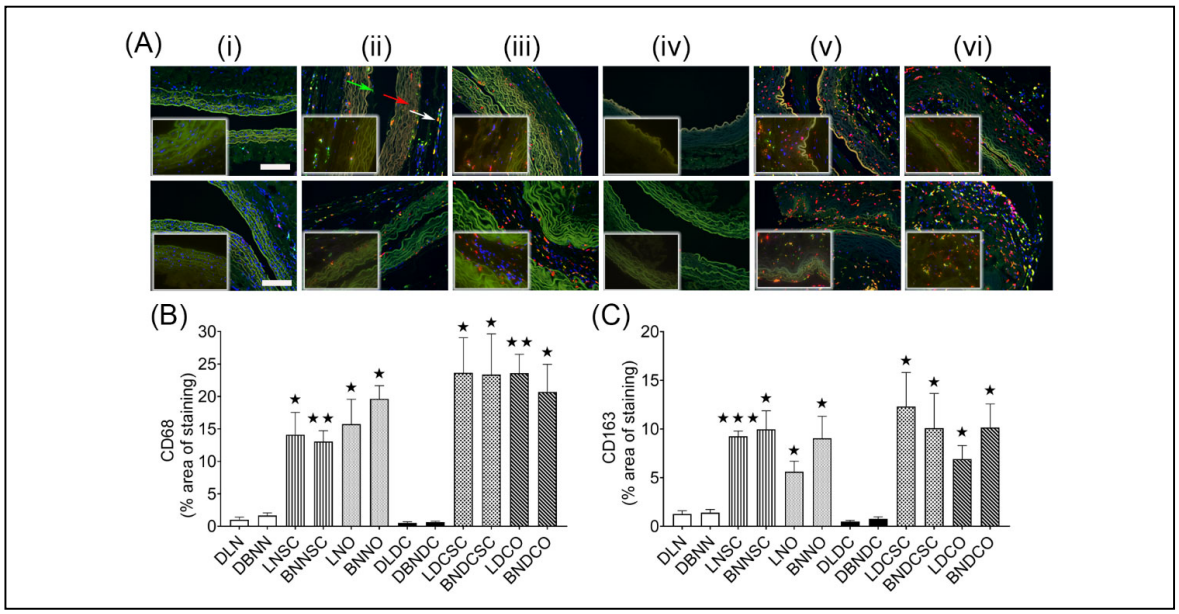

Figure 7. Immunohistostaining identifying macrophage subsets, CD68 and CD163 participating in the host response to implanted aortic scaffolds.

Implants after 2 months' time period were subjected to measurement of macrophage (CD68 and CD163) as outlined in Materials and Methods section. The upper panel denotes the implants from Lewis and the lower panel from Brown Norway rats respectively. **Arrows**- red: CD68 and green: CD163.

7A- Localization and **7B-7D**- Quantification of CD68 and CD163 macrophages.

Data are presented as Mean±SEM (n=6 in each group). Representative images are shown at 20x magnification. Scale bars- 100 µm.

$^{\star}p<0.05$, $^{\star\star}p<0.01$ and $^{\star\star\star}p<0.001$ indicates a significant difference in comparison to the respective donor normal scaffolds by One-way ANOVA followed by Dunnett's T3 Multiple Comparisons post hoc test.

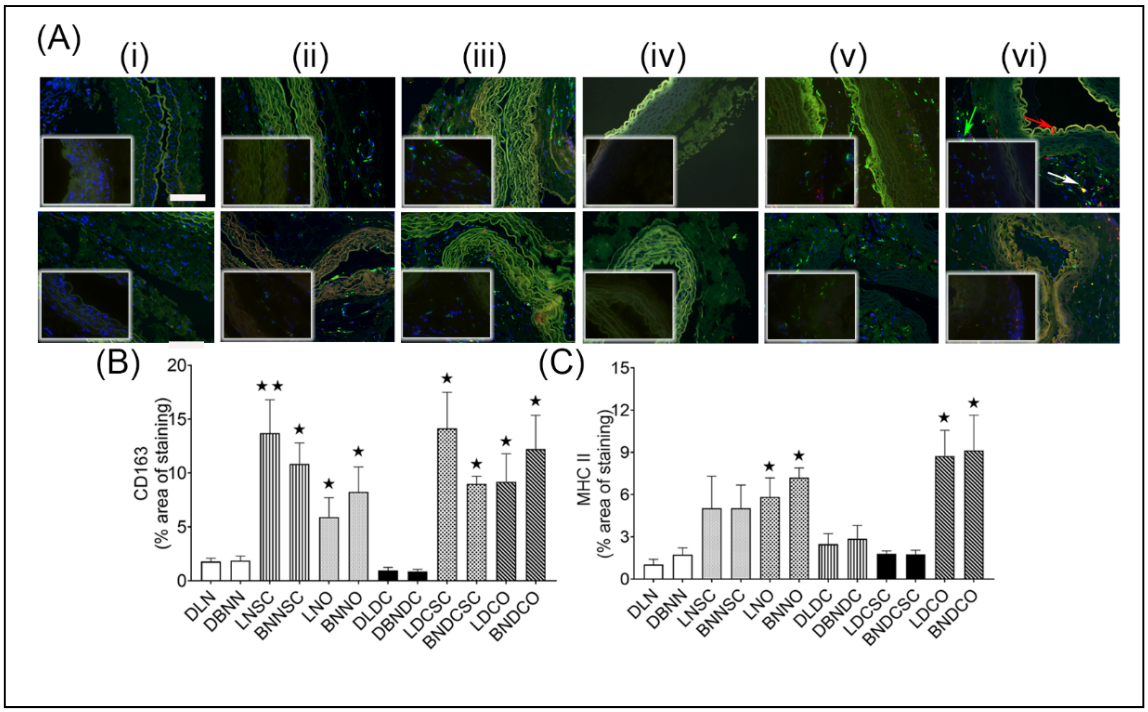

Figure 8. Immunohistostaining identifying macrophage subsets, CD163 and MHCII participating in the host response to implanted aortic scaffolds.

Implanted scaffolds were subjected to immunohistological assessment for different macrophage (CD163 and MHC II) as outlined in Materials and Methods section.

The upper panel denotes the implants from Lewis and the lower panel from Brown Norway rats respectively. **Arrows**- red: MHC II and green: CD163

8A- Localization and **8B-8D**- Quantification of CD163 and MHCII macrophages. Representative images are shown at 20x magnification. Scale bars: 100 µm.

Data are presented as Mean±SEM (n=6 in each group). ★$p<0.05$ and ★★$p<0.01$ indicates a significant difference in comparison to the respective normal normal implants by One-way ANOVA followed by Dunnett's T3 Multiple Comparisons post hoc test.

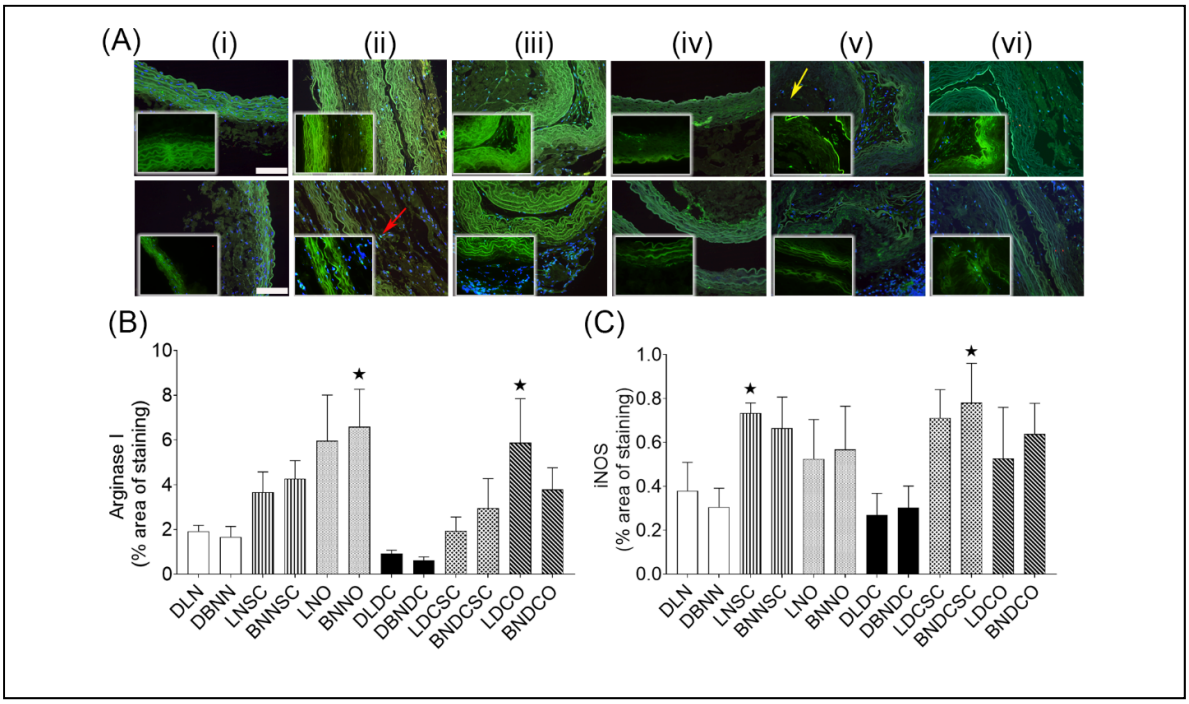

Figure 9. Immunohistostaining identifying macrophage subsets, Arginase I and iNOS participating in the host response to implanted aortic scaffolds.

Implanted scaffolds were subjected to immunohistological assessment for different macrophage (Arginase I and iNOS) as outlined in Materials and Methods section.

The upper panel denotes the implants from Lewis and the lower panel from Brown Norway rats respectively. 9A- Localization and 9B-9C- Quantification of Arginase I and iNOS macrophages. **Arrows**- red: iNOS and green: Arginase I.

Representative images are shown at 20x magnification. Scale bars: 100 µm. Data are presented as Mean±SEM (n=6 in each group). ★$p<0.05$ indicates a significant difference in comparison to the respective normal scaffolds by One-way ANOVA followed by Dunnett's T3 Multiple Comparisons post hoc test.

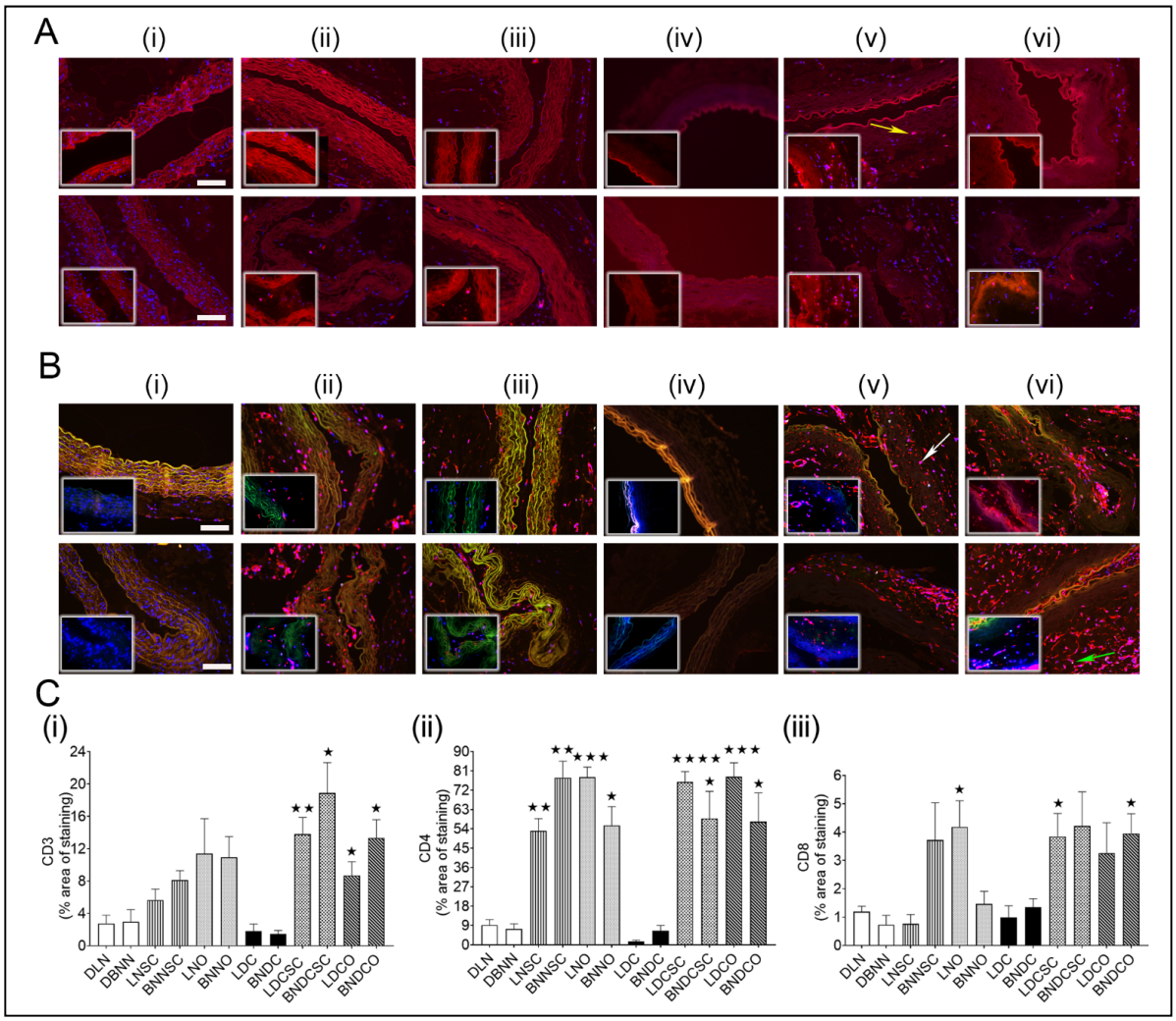

Figure 10. Immunostaining for immune markers, CD3, CD4 and CD8 in the implanted blood vascular scaffolds.

Implanted scaffolds after 2 months' time period were harvested from the subcutaneous and omentum site and analyzed by histological assessment for different immune markers (CD3+, CD4+ and CD8+ cells). The upper panel denotes the implants from Lewis and the lower panel from Brown Norway rats respectively. Yellow arrow denotes the presence of CD3+ve cells, white and green arrow denotes the presence of CD4+ve and CD8+ve cells respectively. Localization **(10A)** and quantification of CD3 (red colour) (**10C i)**; Localization **(10B)** and quantification of CD4 (red colour) and CD8 (green colour) (**10C ii-iii)** is shown.

Representative images are shown at 20x magnification. Scale bars: 100 µm. Data are presented as Mean±SEM (n=6 in each group). ★$p<0.05$, ★★$p<0.01$, ★★★$p<0.001$ and ★★★★$p<0.001$ indicates a significant difference in comparison to the respective normal normal implants by One-way ANOVA followed by Dunnett's T3 Multiple Comparisons post hoc test.

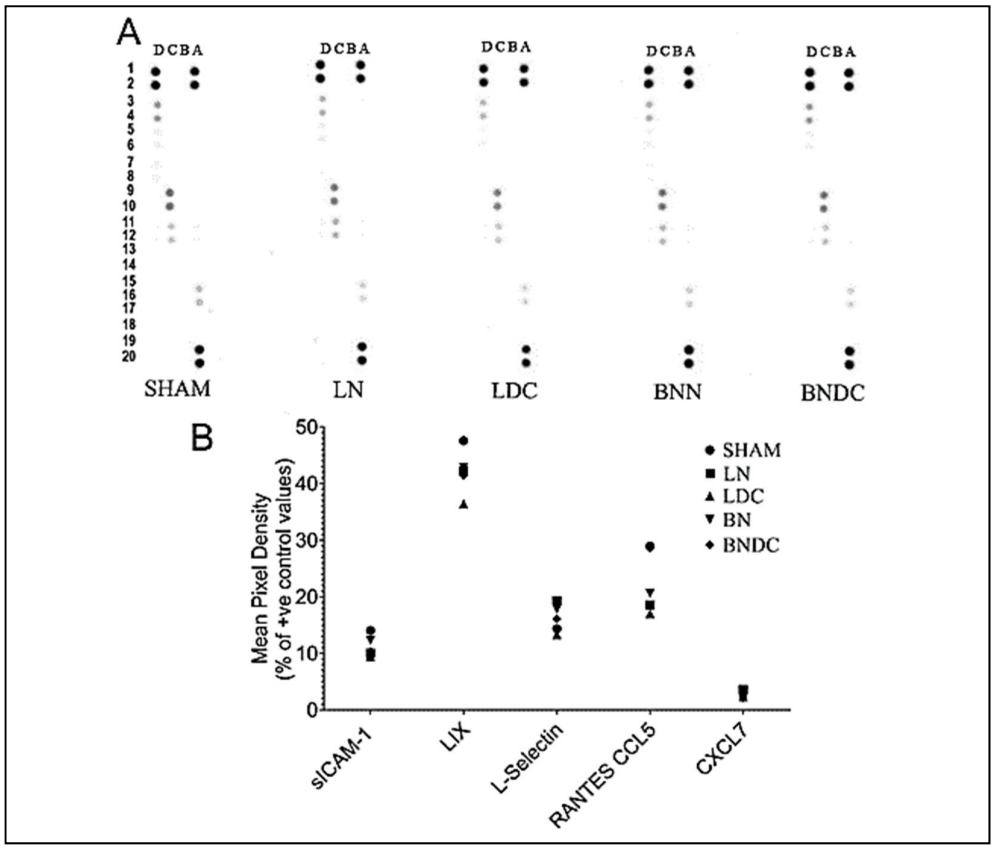

Figure 11. Cytokine and chemokine detection in serum of mice with and without implantation.

A. Membrane based proteome profiling of selected cytokines and chemokines. Serum from implanted recipient Lewis female rats (LN, LDC, BNN and BNDC) was compared with the SHAM operated Lewis female rats and analyzed for the relative level of analytes as specified in the Materials and Methods section.

B. The calculated level of selected analytes showing most prominent expression for all the groups. The relative level of cytokines and chemokines was expressed as Mean Pixel Density after suitable correction of negative and positive reference spots present in the array membrane.

References

1. Weinberg, C. and E. Bell, *A blood vessel model constructed from collagen and cultured vascular cells.* Science, 1986. **231**(4736): p. 397-400.
2. Wu, P., et al., *Construction of vascular graft with circumferentially oriented microchannels for improving artery regeneration.* Biomaterials, 2020. **242**: p. 119922.
3. Burkel, W.E., et al., *Sequential studies of healing in endothelial seeded vascular prostheses: histologic and ultrastructure characteristics of graft incorporation.* J Surg Res, 1981. **30**(4): p. 305-24.
4. Olausson, M., et al., *Transplantation of an allogeneic vein bioengineered with autologous stem cells: a proof-of-concept study.* Lancet, 2012. **380**(9838): p. 230-7.
5. Caralt, M., et al., *Optimization and critical evaluation of decellularization strategies to develop renal extracellular matrix scaffolds as biological templates for organ engineering and transplantation.* Am J Transplant, 2015. **15**(1): p. 64-75.
6. Aamodt, J.M. and D.W. Grainger, *Extracellular matrix-based biomaterial scaffolds and the host response.* Biomaterials, 2016. **86**: p. 68-82.
7. Bloch, O., et al., *Immune response in patients receiving a bioprosthetic heart valve: lack of response with decellularized valves.* Tissue Eng Part A, 2011. **17**(19-20): p. 2399-405.
8. Mendoza-Novelo, B., et al., *Decellularization of pericardial tissue and its impact on tensile viscoelasticity and glycosaminoglycan content.* Acta Biomater, 2011. **7**(3): p. 1241-8.
9. Efendy, J.L., G.R. Campbell, and J.H. Campbell, *The effect of environmental cues on the differentiation of myofibroblasts in peritoneal granulation tissue.* J Pathol, 2000. **192**(2): p. 257-62.
10. Li, J., et al., *Improvement of tracheal autograft survival with transplantation into the greater omentum.* Ann Thorac Surg, 1995. **60**(6): p. 1592-6.
11. Tille, J.C., et al., *Histologic Assessment of Drug-Eluting Grafts Related to Implantation Site.* J Dev Biol, 2016. **4**(1).
12. Hsu, B.R.-S., S.-H. Fu, and A.Y.L. Wang, *Prolonged Survival of Subcutaneous Allogeneic Islet Graft by Donor Chimerism without Immunosuppressive Treatment.* International journal of endocrinology, 2017. **2017**: p. 7057852-7057852.
13. Platell, C., et al., *The omentum.* World J Gastroenterol, 2000. **6**(2): p. 169-176.
14. Smink, A.M., et al., *The Efficacy of a Prevascularized, Retrievable Poly(D,L,-lactide-co-epsilon-caprolactone) Subcutaneous Scaffold as Transplantation Site for Pancreatic Islets.* Transplantation, 2017. **101**(4): p. e112-e119.
15. Anderson, J.M., A. Rodriguez, and D.T. Chang, *Foreign body reaction to biomaterials.* Seminars in Immunology, 2008. **20**(2): p. 86-100.
16. Reid, B., et al., *PEG hydrogel degradation and the role of the surrounding tissue environment.* Journal of Tissue Engineering and Regenerative Medicine, 2015. **9**(3): p. 315-318.
17. Calle, E.A., et al., *Targeted proteomics effectively quantifies differences between native lung and detergent-decellularized lung extracellular matrices.* Acta Biomater, 2016. **46**: p. 91-100.
18. Pan, T.L., et al., *Expression, by functional proteomics, of spontaneous tolerance in rat orthotopic liver transplantation.* Immunology, 2004. **113**(1): p. 57-64.
19. Akhyari, P., et al., *The quest for an optimized protocol for whole-heart decellularization: a comparison of three popular and a novel decellularization technique and their diverse effects on crucial extracellular matrix qualities.* Tissue Eng Part C Methods, 2011. **17**(9): p. 915-26.
20. Crapo, P.M., T.W. Gilbert, and S.F. Badylak, *An overview of tissue and whole organ decellularization processes.* Biomaterials, 2011. **32**(12): p. 3233-43.
21. Gibson-Corley, K.N., A.K. Olivier, and D.K. Meyerholz, *Principles for valid histopathologic scoring in research.* Vet Pathol, 2013. **50**(6): p. 1007-15.
22. Wiśniewski, J.R., et al., *Universal sample preparation method for proteome analysis.* Nat Methods, 2009. **6**(5): p. 359-62.

23. Szklarczyk, D., et al., *STRING v10: protein-protein interaction networks, integrated over the tree of life.* Nucleic Acids Res, 2015. **43**(Database issue): p. D447-52.
24. Shannon, P., et al., *Cytoscape: a software environment for integrated models of biomolecular interaction networks.* Genome Res, 2003. **13**(11): p. 2498-504.
25. Assenov, Y., et al., *Computing topological parameters of biological networks.* Bioinformatics, 2008. **24**(2): p. 282-4.
26. Chin, C.H., et al., *cytoHubba: identifying hub objects and sub-networks from complex interactome.* BMC Syst Biol, 2014. **8 Suppl 4**(Suppl 4): p. S11.
27. Huang da, W., B.T. Sherman, and R.A. Lempicki, *Systematic and integrative analysis of large gene lists using DAVID bioinformatics resources.* Nat Protoc, 2009. **4**(1): p. 44-57.
28. Kanehisa, M., et al., *Data, information, knowledge and principle: back to metabolism in KEGG.* Nucleic Acids Res, 2014. **42**(Database issue): p. D199-205.
29. McDermott, G.P., et al., *Multiplexed target detection using DNA-binding dye chemistry in droplet digital PCR.* Anal Chem, 2013. **85**(23): p. 11619-27.
30. Coulter, S.J., *Mitigation of the effect of variability in digital PCR assays through use of duplexed reference assays for normalization.* Biotechniques, 2018. **65**(2): p. 86-91.
31. Perez-Riverol, Y., et al., *The PRIDE database and related tools and resources in 2019: improving support for quantification data.* Nucleic Acids Res, 2019. **47**(D1): p. D442-d450.
32. Tondreau, M.Y., et al., *Mechanical properties of endothelialized fibroblast-derived vascular scaffolds stimulated in a bioreactor.* Acta Biomater, 2015. **18**: p. 176-85.
33. Brasile, L., et al., *Pretransplant Kidney-Specific Treatment to Eliminate the Need for Systemic Immunosuppression.* Transplantation, 2010. **90**: p. 1294-8.
34. Methe, K.N., et al., *Differential Activation of Immune Cells for Genetically Different Decellularized Cardiac Tissues.* Tissue Eng Part A, 2020.
35. Schmitt, A., et al., *Optimized protocol for whole organ decellularization.* European Journal of Medical Research, 2017. **22**(1): p. 31.
36. Heath, D.E., *A Review of Decellularized Extracellular Matrix Biomaterials for Regenerative Engineering Applications.* Regenerative Engineering and Translational Medicine, 2019. **5**(2): p. 155-166.
37. Coito, A.J., et al., *The expression of extracellular matrix proteins during accelerated rejection of cardiac allografts in sensitized rats.* Transplantation, 1994. **57**(4): p. 599-605.
38. Black, F.M., et al., *The vascular smooth muscle alpha-actin gene is reactivated during cardiac hypertrophy provoked by load.* J Clin Invest, 1991. **88**(5): p. 1581-8.
39. Lambris, J.D., K.B. Reid, and J.E. Volanakis, *The evolution, structure, biology and pathophysiology of complement.* Immunol Today, 1999. **20**(5): p. 207-11.
40. Ricklin, D., et al., *Complement: a key system for immune surveillance and homeostasis.* Nat Immunol, 2010. **11**(9): p. 785-97.
41. Lin, C.M. and R.G. Gill, *Direct and indirect allograft recognition: pathways dictating graft rejection mechanisms.* Curr Opin Organ Transplant, 2016. **21**(1): p. 40-4.
42. Mills, C.D., et al., *M-1/M-2 macrophages and the Th1/Th2 paradigm.* J Immunol, 2000. **164**(12): p. 6166-73.
43. Juhas, M., et al., *Incorporation of macrophages into engineered skeletal muscle enables enhanced muscle regeneration.* Nature Biomedical Engineering, 2018. **2**(12): p. 942-954.
44. Graney, P.L., et al., *Macrophages of diverse phenotypes drive vascularization of engineered tissues.* Sci Adv, 2020. **6**(18): p. eaay6391.
45. Creemers, P., et al., *Evaluation of peripheral blood CD4 and CD8 lymphocyte subsets, CD69 expression and histologic rejection grade as diagnostic markers for the presence of cardiac allograft rejection.* Transpl Immunol, 2002. **10**(4): p. 285-92.
46. Gu, H., et al., *Bone regeneration in a rabbit ulna defect model: use of allogeneic adipose-derivedstem cells with low immunogenicity.* Cell Tissue Res, 2014. **358**(2): p. 453-64.

47. Piccotti, J.R., et al., *Are Th2 helper T lymphocytes beneficial, deleterious, or irrelevant in promoting allograft survival?* Transplantation, 1997. **63**(5): p. 619-24.
48. Zaiss, D.M., et al., *Amphiregulin enhances regulatory T cell-suppressive function via the epidermal growth factor receptor.* Immunity, 2013. **38**(2): p. 275-84.
49. Arpaia, N., et al., *A Distinct Function of Regulatory T Cells in Tissue Protection.* Cell, 2015. **162**(5): p. 1078-89.
50. Vlahos, A.E., N. Cober, and M.V. Sefton, *Modular tissue engineering for the vascularization of subcutaneously transplanted pancreatic islets.* Proc Natl Acad Sci U S A, 2017. **114**(35): p. 9337-9342.
51. Berman, D.M., et al., *Long-term survival of nonhuman primate islets implanted in an omental pouch on a biodegradable scaffold.* Am J Transplant, 2009. **9**(1): p. 91-104.
52. Brown, B.N., et al., *Macrophage phenotype and remodeling outcomes in response to biologic scaffolds with and without a cellular component.* Biomaterials, 2009. **30**(8): p. 1482-91.
53. Brown, B.N., et al., *Macrophage phenotype as a predictor of constructive remodeling following the implantation of biologically derived surgical mesh materials.* Acta Biomater, 2012. **8**(3): p. 978-87.
54. Gilbert, T.W., T.L. Sellaro, and S.F. Badylak, *Decellularization of tissues and organs.* Biomaterials, 2006. **27**(19): p. 3675-83.
55. Naso, F., et al., *Are FDA and CE sacrificing safety for a faster commercialization of xenogeneic tissue devices? Unavoidable need for legislation in decellularized tissue manufacturing.* Tissue Antigens, 2014. **83**(3): p. 193-4.